Benzyl and Benzoyl Benzoic Acid Inhibitors of Bacterial RNA Polymerase-Sigma Factor Interaction

Jiqing Ye [a,1], Adrian Jun Chu [b,1], Lin Lin [b], Shu Ting Chan [a], Rachel Harper [b], Min Xiao [c], Irina Artsimovitch [d], Zhong Zuo [c], Cong Ma [a,], Xiao Yang [b,*]*

[a] State Key Laboratory of Chemical Biology and Drug Discovery, Department of Applied Biology and Chemical Technology, The Hong Kong Polytechnic University, Hung Hom, Kowloon, Hong Kong SAR

[b] Department of Microbiology, The Chinese University of Hong Kong, Prince of Wales Hospital, Shatin, Hong Kong SAR

[c] School of Pharmacy, Faculty of Medicine, The Chinese University of Hong Kong, Shatin, New Territories, Hong Kong SAR

[d] Department of Microbiology and The Center for RNA Biology, The Ohio State University, Columbus, OH 43210, USA

Abstract

Transcription is an essential biological process in bacteria requiring a core enzyme, RNA polymerase (RNAP). Bacterial RNAP is catalytically active but requires sigma (σ) factors for transcription of natural DNA templates. σ factor binds to RNAP to form a holoenzyme which specifically recognizes a promoter, melts the DNA duplex, and commences RNA synthesis. Inhibiting the binding of σ to RNAP is expected to inhibit bacterial transcription and growth. We previously identified a triaryl hit compound that mimics σ at its major binding site of RNAP, thereby inhibiting the RNAP holoenzyme

formation. In this study, we modified this scaffold to provide a series of benzyl and benzoyl benzoic acid derivatives possessing improved antimicrobial activity. A representative compound demonstrated excellent activity against *Staphylococcus epidermidis* with minimum inhibitory concentrations reduced to 0.5 µg/mL, matching that of vancomycin. The molecular mechanism of inhibition was confirmed using biochemical and cellular assays. Low cytotoxicity and metabolic stability of compounds demonstrated the potential for further studies.

1. Introduction

Bacterial infectious diseases pose serious problems to human health and the economy. The World Health Organization published a priority pathogen list for guiding the R&D of antibiotics in 2017 [1]. Bacterial transcription is a valid but underutilized target for antimicrobial agent discovery; rifamycins and fidaxomicin are the only two types of antibiotics used in clinics that target bacterial RNA polymerase (RNAP) [2].

Bacterial RNAP core enzyme composed of five subunits (α dimer, β, β' and ω) is capable of RNA synthesis on synthetic single-stranded DNA templates but requires accessory σ factors to initiate transcription at promoters (Figure 1A) [3]. Bacterial σ factor binds to RNAP to form a holoenzyme, specifically recognizes promoter DNA elements, and triggers DNA strand separation to expose the transcription start site to initiate RNA synthesis [4, 5]. Housekeeping σ factors (named σ^A in most bacteria, σ^{70} in *Escherichia coli*) required for transcription of most genes are highly conserved and

essential for cell functions and viability [6-8]. Determination of high-resolution structures of RNAP holoenzyme complexes [9, 10] paved a road toward the structure-guided discovery of antimicrobial agents targeting the RNAP-σ interaction.

The interactions between the clamp helices (CH) domain of the RNAP β' subunit and σ^{70} region 2.2 are thought to play a dominant role in the holoenzyme formation [11, 12]. Focusing on key amino acid residues at the β'CH-$\sigma_{2.2}$ interface (Figure 1B), we designed a pharmacophore model and carried out *in silico* screening for protein-protein (PPI) inhibitors [13, 14]. The first generation of bis-indole inhibitor compounds exhibited mild broad-spectrum antimicrobial activity with confirmed mechanism and specificity (i.e., targeting β'CH) [13], as did the second generation of inhibitors with more drug-like properties [15]. Small-molecule inhibitors of RNAP-σ interaction have also been identified by screening compounds for inhibition of *E. coli* RNAP-σ^{70} binding *in vitro* and by virtual screening of a pharmacophore model based on structures of bioactive compounds with unknown or diverse binding sites on RNAP [16, 17]. However, the exact binding sites of these compounds remain to be elucidated.
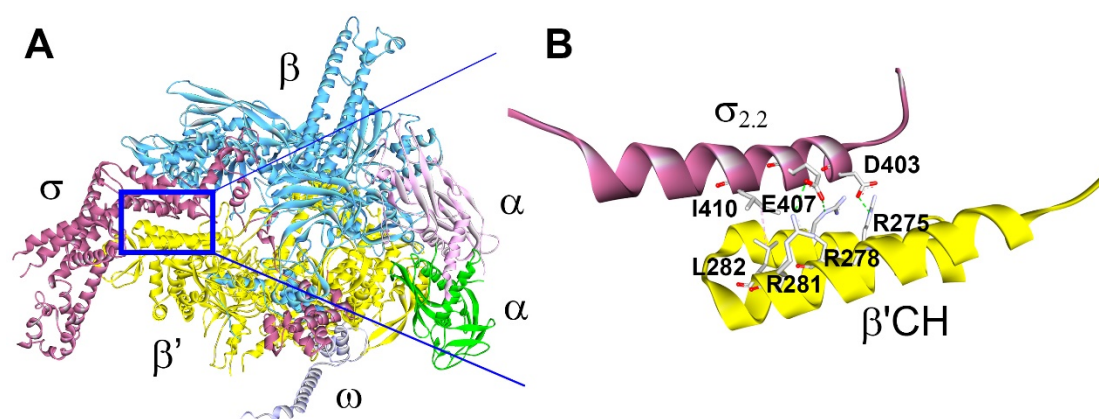

Fig. 1. Structure of A) the *E. coli* RNAP holoenzyme crystal complex (PDB: 4LJZ) and B) interactions at the interface of $\sigma_{2.2}$ and β'CH, with key amino acid side chains shown [18].

We were particularly interested in a triaryl **C3** compound (Fig. 2A) due to its drug-like properties and the presumed efficiency of structure modification. Using the ELISA-based inhibitory assay and the protein complement assay, we have confirmed that **C3** specifically inhibited the β'CH-σ interaction *in vitro* [15][19]. **C3** displayed mild antimicrobial activity against *Streptococcus pneumoniae* ATCC 49619 with a minimum inhibitory concentration (MIC) of 256 µg/mL. Preliminary structural optimizations of **C3** were carried out in previous studies [20]. We first investigated the contribution of the left benzene ring while keeping the right benzoic acid moiety intact, because the latter was predicted to form strong ionic bonds to two β' arginine residues R278 and R281 (*E. coli* numbering) (Fig. 2B) [20]. A simple modification from 2-aminobenzene to 3,4-dichlorobenzene resulted in **C3-005** (Fig. 2A), which significantly improved the antimicrobial activity against *S. pneumoniae* to an MIC of 8 µg/mL (Fig. 2A); in addition, the **C3-005** inhibitory effects on *S. pneumoniae* toxin production were comparable to those of antibiotics currently on the market [20].
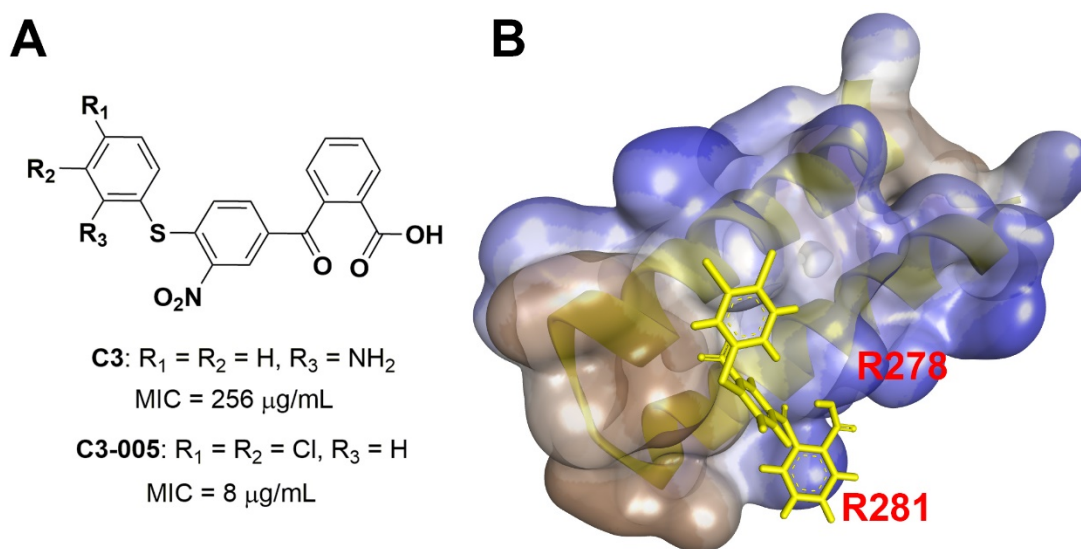

Fig. 2. A) Structures of **C3** and **C3-005** and MICs against *S. pneumoniae*; B) Docking model of **C3-005** (yellow) onto β'CH (semi-transparent surface showing hydrophobicity in blue).

2. Results and discussion
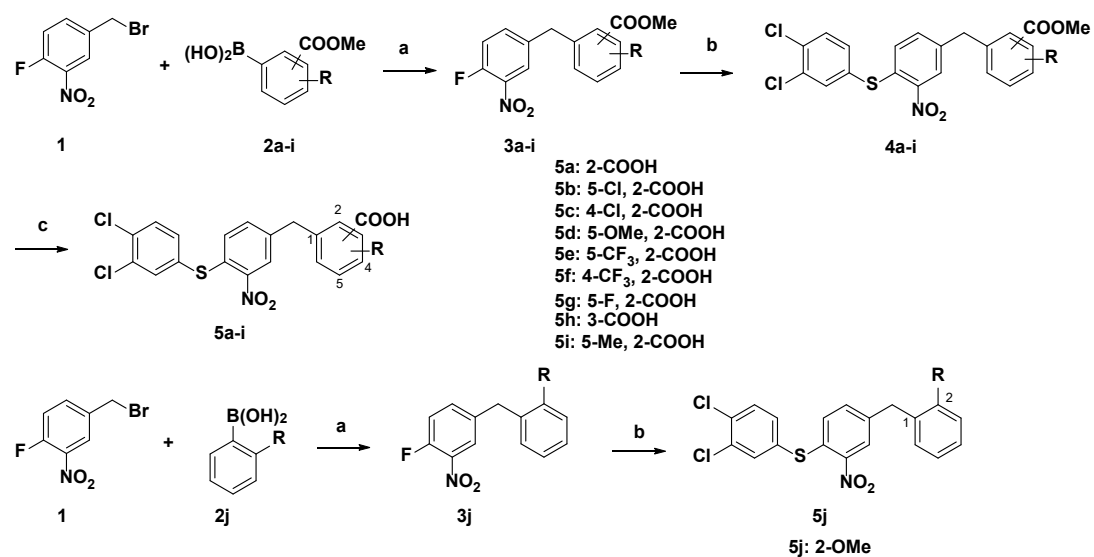
2.1. Design of benzyl and benzoyl derivatives

In this study, we intended to modify the right benzoyl benzoic acid motif to explore the appropriate chemical space required for binding to the β'CH and the resulting changes in the antimicrobial activity. According to the pharmacophore docking model, the right benzoic acid in **C3-005** is pincered by the β'CH residues R278 and R281 (Figure 1B & 2B). Therefore, starting with **C3-005** as the lead compound, we intended to explore the substituents on the right benzene ring and test their effects on the antimicrobial activity. Additionally, we wished to verify the importance of benzoic acid for activity by using modifications to other functional groups.

In **C3-005**, the benzoyl group is bound to benzoic acid to maintain a quasi-planar conformation of the right part of the molecule (Fig. 2B). We were also interested in determining whether a flexible conformation would make a difference, by modifying benzoyl to benzyl with a methylene group replacing carbonyl despite possible existence of hyperconjugation in a diphenylmethane type of structure.

2.2 Chemistry

As shown in Scheme 1, compounds **5a** – **j** were synthesized. Suzuki coupling of 4-(bromomethyl)-1-fluoro-2-nitrobenzene **1** with arylboronic acids **2a** – **j** provided **3a** – **j** [21]. Substitution of the fluoride group with 3,4-dichlorobenzenethiol gave thiol ethers **4a** – **i**, and **5j**. The methyl benzoates were then hydrolyzed with aqueous solution of sodium hydroxide to yield benzoic acids **5a** – **i**.
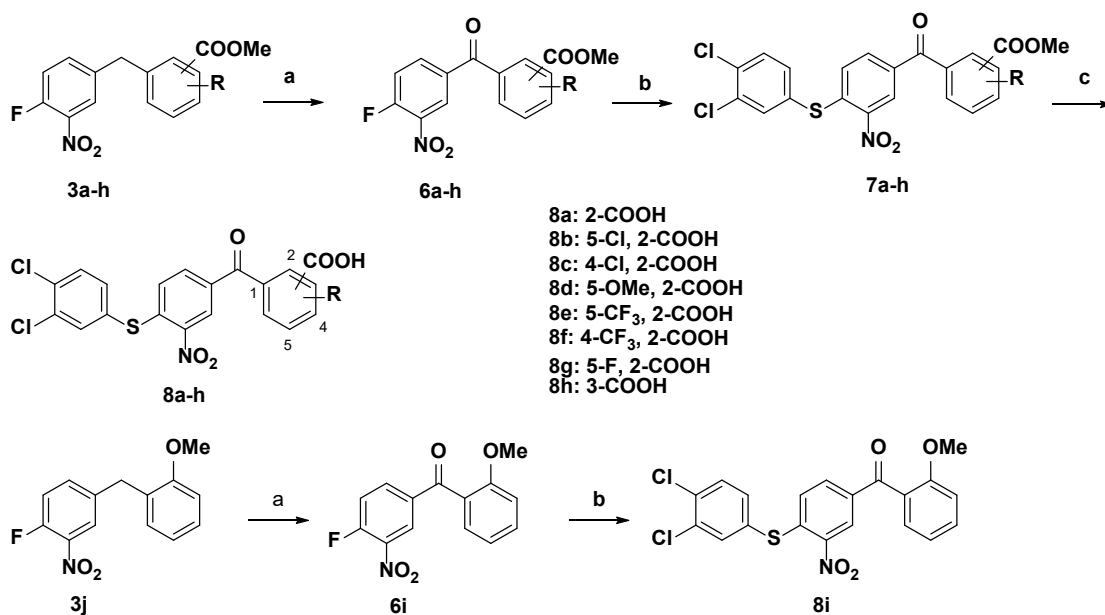
Scheme 1. Synthetic route for compounds **5a** – **j**[a]

5a: 2-COOH
5b: 5-Cl, 2-COOH
5c: 4-Cl, 2-COOH
5d: 5-OMe, 2-COOH
5e: 5-CF$_3$, 2-COOH
5f: 4-CF$_3$, 2-COOH
5g: 5-F, 2-COOH
5h: 3-COOH
5i: 5-Me, 2-COOH

5j: 2-OMe

[a] Reagents and conditions: a) Arylboronic acid, Pd(OAc)$_2$, PPh$_3$, K$_3$PO$_4$, Tol, 80 °C; b) 3,4-Dichlorobenzenethiol, NaOAc, EtOH, reflux; (c) NaOH, H$_2$O, dioxane, 50 °C, overnight.

The intermediates **3a** – **h** and **3j** were subjected to synthesis of **8a** – **i** (Scheme 2). Oxidation of **3a** – **h** and **3j** provided diarylketones **6a** – **i** employing NBS [22]. Thioethers **7a** – **h** and **8i** were prepared by substitution of fluoride with 3,4-dichlorobenzenethiol as described above. After hydrolysis of esters, benzoic acids **8a** – **h** were obtained.

Scheme 2. Synthetic route for compounds **8a** – **i**[a]

3a-h → a → 6a-h → b → 7a-h → c →

8a: 2-COOH
8b: 5-Cl, 2-COOH
8c: 4-Cl, 2-COOH
8d: 5-OMe, 2-COOH
8e: 5-CF$_3$, 2-COOH
8f: 4-CF$_3$, 2-COOH
8g: 5-F, 2-COOH
8h: 3-COOH

8a-h

3j → a → 6i → b → 8i

^{a} Reagents and conditions: (a) NBS, H$_2$O, CHCl$_3$, 60 ~ 85 °C; (b) 3,4-Dichlorobenzenethiol, NaOAc, EtOH, reflux; (c) NaOH, H$_2$O, dioxane, 50 °C, overnight.

2.3 Microbiological assessment

2.3.1 Antimicrobial activities

The in-house synthesized compounds **5a – j** and **8a – i** were tested for their antimicrobial activities against *S. pneumoniae* and *Staphylococcus aureus*, both of which are on the WHO priority pathogen list for R&D of new antibiotics [23]. As shown in Table 1, the antimicrobial activities of all the 4- or 5-substituted 2-benzoic acids were significantly improved against all the bacteria tested when electron-withdrawing substituents (**8b – c, 8e – f**) were present, as compared to **8a**. The greatest activity was observed when the structure contains 5-trifluoromethyl-2-benzoic acid (**8e**). Electron-donating group (**8d**) and fluoride (**8g**) maintained the antimicrobial activity against *S. pneumoniae* and *S. aureus* ATCC 25923, and slightly improved activity against *S. aureus* ATCC 29213. Note that compounds **8b – c, 8e – f** were predicted to possess
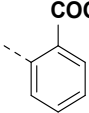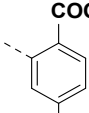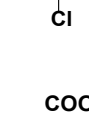
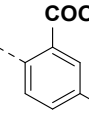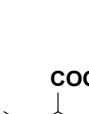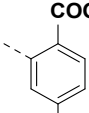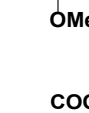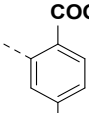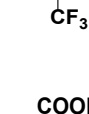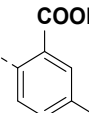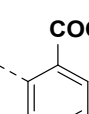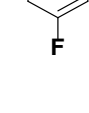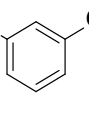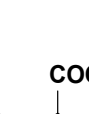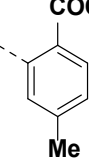slightly higher clogP values than **8a**, **8d**, and **8g**. These results suggest that additional substituents may increase the binding to the protein surface, which is favorable for activity. Membrane permeability may also play a role in increasing cellular compound concentration.
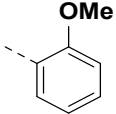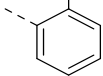
Compounds **5a** – **g** and **5i** with benzyl benzoic acid moiety demonstrated a similar trend but slightly superior antimicrobial activity as compared to benzoyl benzoic acid analogues **8a** – **g**, probably due to a more flexible structure and slightly higher clogP values (Table 1). Again, all of the electron-withdrawing (**5b** – **c**, **5e** – **f**) and -donating groups (**5d** and **5i**) substituted on the right benzene ring of **5a** improved the antimicrobial activity. In particular, trifluoromethyl substituted compound **5e** exhibited an MIC of 1 μg/mL against *S. pneumoniae*, even though being eight times less potent against *S. aureus*.

When the benzoic acid group was moved to 3-position (**5h** and **8h**) or changed to methoxy (**5j** and **8i**), the antimicrobial activity vanished. The docking model (Fig. 2B) demonstrates that the benzoic acid group at 2-position to benzyl or benzoyl is positioned between β'CH R278 and R281. The experimental results suggest that benzoic acid may form a critical ionic bonding interaction with the binding site at β'CH, and that the relative position of benzoic acid to the core structure of inhibitor is also influenced by modifications.

Table 1. Antimicrobial activity and clogP values of synthesized compounds

No.	R	MIC (μg/mL)			clogP
		SPNE	SAUR[a]	SAUR[b]	
5a		16	16	16	6.59

Compound	Structure				
8a (C3-005)	COOH (benzoic acid)	8	16	16	5.94
5b	COOH, Cl	2	8	8	7.40
8b		8	8	8	6.69
5c	COOH, Cl	4	8	8	7.40
8c		8	8	4	6.69
5d	COOH, OMe	8	16	8	6.72
8d		8	16	8	6.04
5e	COOH, CF$_3$	1	8	8	7.64
8e		2	4	4	6.87
5f	COOH, CF$_3$	2	16	8	7.64
8f		4	16	8	6.87
5g	COOH, F	4	8	8	6.83
8g		8	16	8	6.12
5h	COOH	>256	>256	>256	7.49
8h		>256	>256	32	6.74
5i	COOH, Me	4	4	4	7.08

| 5j | OMe | >256 | >256 | >256 | 7.66 |
| 8i | | >256 | >256 | >256 | 6.98 |

SPNE: *S. pneumoniae* ATCC 49619, SAUR[a]: *S. aureus* ATCC 25923, SAUR[b]: *S. aureus* ATCC 29213

Since compound **8e** demonstrated good antimicrobial activity against *S. aureus* and *S. pneumoniae* with MICs of 2 – 4 μg/mL (Table 1), we went on to further assess its potency against a representative panel of clinically significant Gram-positive pathogens. Growth of both Group A *Streptococcus* (*Streptococcus pyogenes;* GAS) causing strep throat, localized skin infection and necrotizing fasciitis [24] and Group B *Streptococcus* (*Streptococcus agalactiae;* GBS) causing neonatal infections [25] was inhibited by compound **8e,** with MIC 4 μg/mL (Fig. 3). Responsible for serious opportunistic infections, other staphylococcal strains (*Staphylococcus epidermidis* and *S. Staphylococcus saprophyticus*) were particularly sensitive when challenged by **8e,** with MICs reaching 0.5 – 1 μg/mL, a level comparable to the last-resort antibiotic vancomycin (Fig. 3). Several clinically significant Gram-negative pathogens were also tested, but none was inhibited by the compounds (data not shown). This could result from the difference in membrane permeability and efflux mechanisms between Gram-positive and -negative bacteria.

No.	EFAE	SEPI	SSAP	SPYO	SAGA	CDIFF	RT 002	RT 027
8e	8	0.5	1	4	4	8	8	8
VAN	1	0.5	0.25	1	2	4	2	2

Fig. 3. Antimicrobial activity (MIC μg/mL) of compound **8e** against clinically important Gram-positive pathogens. EFAE: *Enterococcus faecalis* ATCC 19433, SEPI: *S. epidermidis* ATCC 12228, SSAP: *S. saprophyticus* ATCC 15305, SPYO: *S. pyogenes*

ATCC 19615, SAGA: *S. agalactiae* ATCC 12386, CDIFF: *Clostridium difficile* ATCC 9689; RT 002: *C. difficile* ribotype 002; RT 027: *C. difficile* ribotype 027; VAN: vancomycin.

Clostridium difficile infections (CDIs) cause diarrhoea in adults and burden the global healthcare system [26, 27]. The clinical outlook is further complicated by the prevalence of the hypervirulent strain ribotype 027 (B1/NAP1/027) in Europe and the USA [28, 29], whilst ribotype 002 is associated with high mortality frequently reported in Asia-Pacific region such as Hong Kong [30, 31]. Current treatment of severe CDIs includes narrow-spectrum drugs such as vancomycin, whilst newer options such as rifampicin and fidaxomicin have emerged for the management of serious recurrent CDIs [32]. Since both rifampicin and fidaxomicin act by inhibiting bacterial transcription [33], **8e** was also assessed for its possible role as an anti-clostridial agent. In our study, we included the historical non-NAP1 isolate *C. difficile* ATCC 9689 as a type strain, alongside the virulent isolate ribotype 002 and the hypervirulent strain ribotype 027. All three clostridial strains responded reasonably well to **8e** when exposed for 48 hours anaerobically (MIC = 8 μg/mL; Fig. 3), which incentivized further investigations into the potential effects of **8e** on clostridial virulence.

2.3.2 C. difficile toxin secretion

Production of cytotoxins Toxin A (TcdA) and Toxin B (TcdB) are thought to contribute towards *C. difficile* hypervirulence [34-36]. Fidaxomicin, which inhibits bacterial transcription initiation, has been shown to suppress toxin production in *C. difficile* strains when compared with first-line anti-clostridial drugs such as vancomycin and metronidazole [37, 38]. Therefore, we compared anti-clostridial effects of our

compound **8e,** which also inhibits transcription initiation, to those of vancomycin and fidaxomicin by assessing *C. difficile* viable colony counts and measuring toxin attenuation. Typically, both Toxins A and B undergo optimal production during the stationary phase of *C. difficile*, and their release can be accelerated under conditions of stress, such as chemotherapeutic challenges [39, 40]. *C. difficile* strains were therefore cultured and incubated anaerobically in the presence of sub-inhibitory concentrations of compound **8e**, vancomycin and fidaxomicin for up to 48 hours, whereby the levels of Toxins A and B can be determined and cross-referenced with counts of colony-forming units (CFUs).

A 9689

B 002

C 027
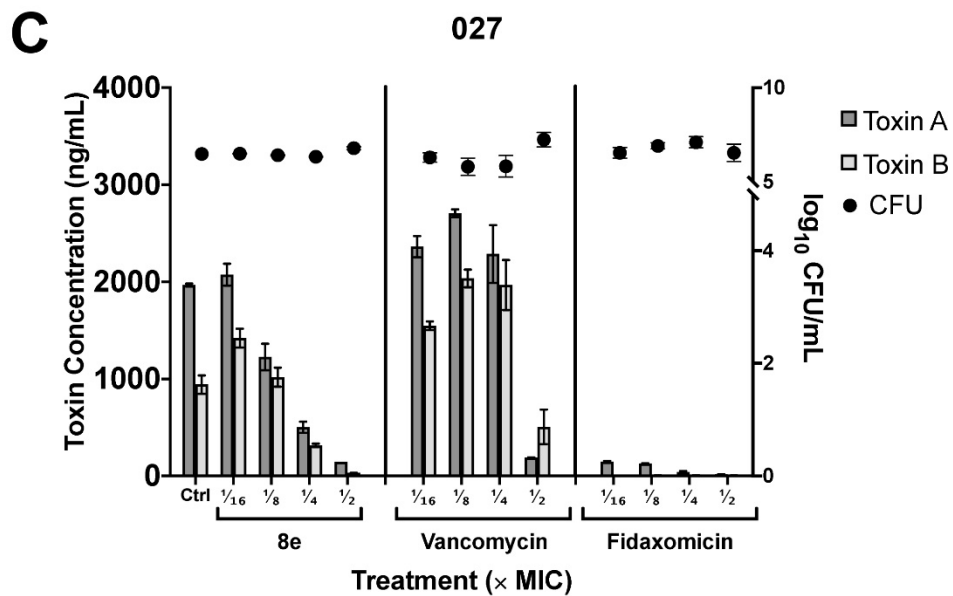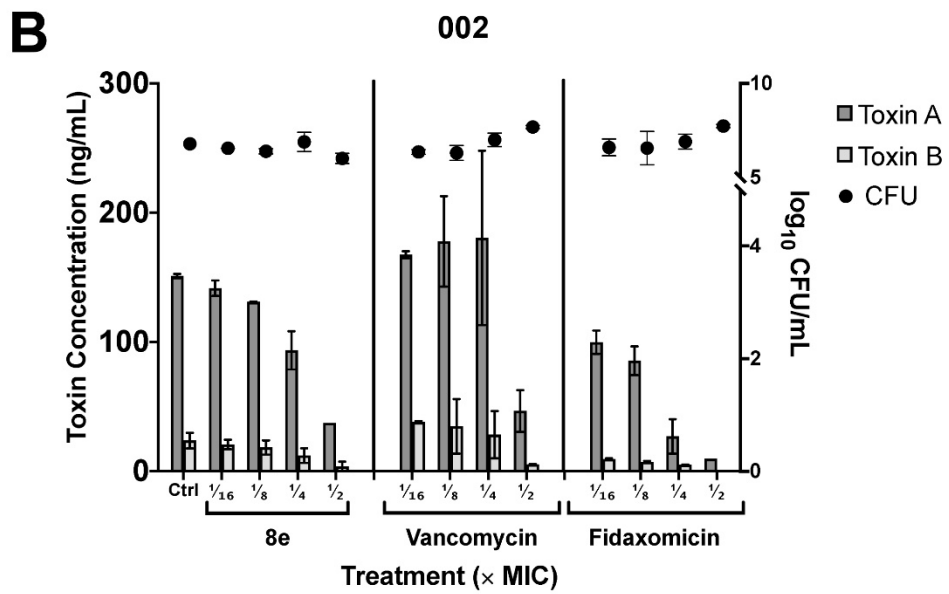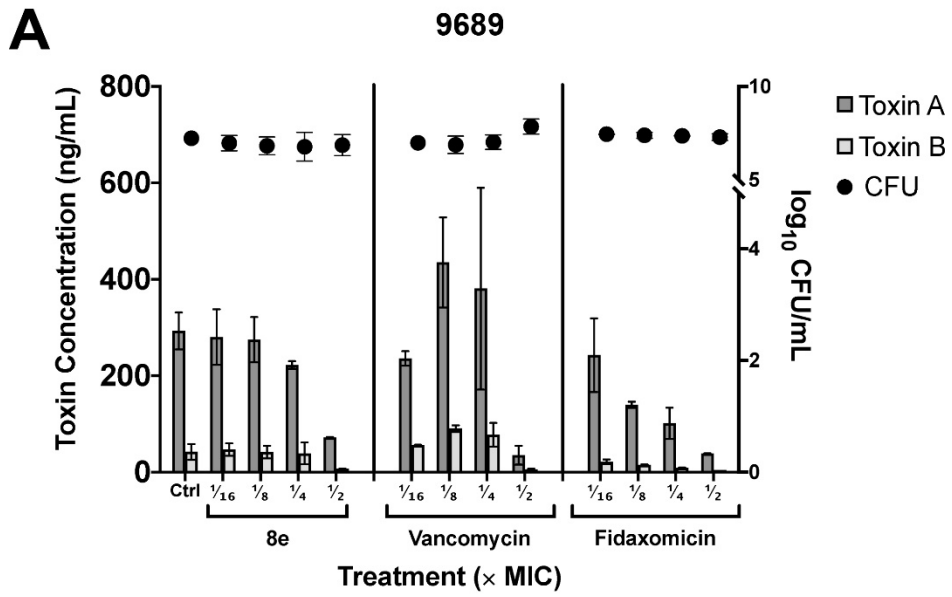
Fig. 4. Effects of test compound **8e** and control drugs vancomycin and fidaxomicin at sub-inhibitory concentrations (1/2 ×, 1/4 ×, 1/8 ×, and 1/16 × MIC) on the levels of Toxin A (dark grey bars), Toxin B (light grey bars) and CFU count (black circles) in (**A**) *C. difficile* ATCC 9689, (**B**) ribotype 002, and (**C**) ribotype 027 after 48 hours of anaerobic incubation. All toxin levels were normalized against drug-free control (dotted horizontal line from left y-axis = 1). CFU counts are relative to drug-free control values denoted by each respective dashed horizontal line from right y-axes: (**A**) y = 7.23, (**B**) y = 6.79 and (**C**) y = 6.48.

The results revealed that the effects of transcription inhibitors were different from those of vancomycin, which inhibits cell wall biosynthesis (Fig. 4). When present at low concentrations, vancomycin stimulated toxin production, and inhibition was observed only at ½ MIC; this stimulation may be plausibly attributed either to upregulation of exotoxin gene expression by vancomycin, as reported for some genes in *S. aureus* [41], or to the inadvertent mechanical disruption of clostridial cell walls upon inhibition of their biosynthesis by vancomycin. The lytic release of toxins is supported by the drop in viable cell counts in all three strains treated with decreasingly sublethal doses of vancomycin being contrasted with increasing levels of Toxins A and B detected in supernatants. By contrast, the test compound **8e** and fidaxomycin inhibited the release of Toxins A and B in all three *C. difficile* strains at subinhibitory concentrations in a dose-dependent manner (Fig. 4). Fidaxomicin demonstrated remarkable toxin-suppressing potency even at more diluted concentrations, especially against the hypervirulent ribotype 027 (Fig. 4C). **8e** could, however, largely match the effects of fidaxomicin when its concentration was further increased, for example, to ½ × MIC across all three strains.

2.4. Mechanistic studies:

2.4.1 In vitro β'CH - σ affinity inhibitory assay

Selected compounds **5b**, **5e**, **8e**, and **5f** were also examined for their inhibitory activity against *in vitro* interaction between β'CH and σ, using the previously established NanoLuc protein complementation assay (PCA) [19]. The PPI pair consisted of a combination of C-LgBiT-σ^A and C-SmBiT-β'CH close to a 1:1 ratio, which generated luminescence unless prevented from binding by a test compound. We incubated the PPI pair with increasing concentrations of test compounds and plotted a dose-dependent decrease in luminescence, which was expressed as a percentage of inhibition of β'CH-σ as compared to the no-drug control (Fig. 5). We found that compounds **5b**, **5e**, and **8e** showed good inhibitory activity, implying that their binding to the β'CH/σ interface was preserved following structural modifications to the lead compound **8a** through the addition of Cl or trifluoromethyl (CF$_3$) groups (Table 1 and Fig. 5). **5b**, **5e**, and **8e** significantly decreased luminescence at relatively low concentrations, whereas **5f** was less potent (Fig. 5). Comparison of **5b**, **5e**, and **8e** with **5f** suggests that the substitution of Cl or CF$_3$ at the *para*-position of benzoic acid significantly improved the bonding interaction of benzoic acid with β'CH R278 and R281, and thus increased their inhibitory activity.
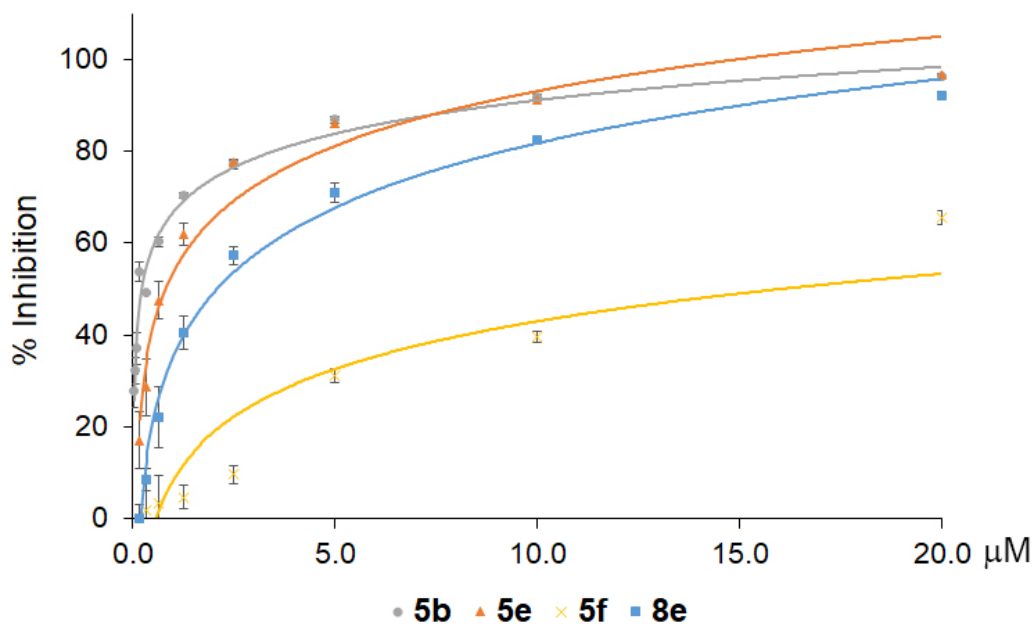
Fig. 5. Inhibition of the β'CH-σ interaction by representative compounds **5b**, **5e**, **8e** and **5f** using the NanoLuc PCA system.

The half-inhibitory activity (IC_{50}) of β'CH-σ interaction was calculated for compounds **5b**, **5e**, **8e** and **5f** and presented in Table 2. The IC_{50} for the compounds corresponded to their antimicrobial activities, especially for **5f**, which has the highest IC_{50} and MIC values against *S. pneumoniae* (Tables 1 and 2). However, inhibition of target protein function, or in this case protein-protein interactions, is not the sole determinant of *in vitro* antimicrobial activities. There are a number of other contributing factors, such as solubility, membrane permeability, modification/degradation by bacterial enzyme, and efflux. Based on its potent antimicrobial activity (Table 1 and Fig. 3) and efficient inhibition β'CH-σ interaction (Fig. 5), compound **8e** was chosen for further mechanistic studies.

Table 2. IC_{50} of representative compounds inhibiting the β'CH-σ interaction

No.	5b	5e	5f	8e
IC$_{50}$ (µM)	0.26 ± 0.04	0.73 ± 0.04	16.00 ± 0.04	2.12 ± 0.21

2.4.2. Confocal fluorescence microscope

The cellular effects of compound **8e** were examined by fluorescent microscopy as previously described [14]. *B. subtilis* strain BS1048 carries a *gfp*-fused *rpoC* gene expressing the green fluorescence protein (GFP)-tagged β' subunit of RNAP. As expected, fluorescently tagged RNAP localized to the central chromosome-containing lumen of the cell in the untreated control strain (Fig. 6 Ctrl; [42]). **8e** elicited antimicrobial activity against *B. subtilis* BS1048 with a MIC of 2 µg/mL. When **8e** was added at ½ MIC, fluorescence was seen to have delocalized from the nucleoid compared to the untreated control, which may be a result of decondensed chromosomes at the sub-MIC levels (Fig. 6 ½ MIC). As the concentration of **8e** was increased, diffusion of the fluorescent signal into the cytosol became more pronounced (Fig. 6 1 MIC and 2 MIC). These results suggest that **8e** can affect the localization of bacterial transcription complexes when assessed at the cellular level.
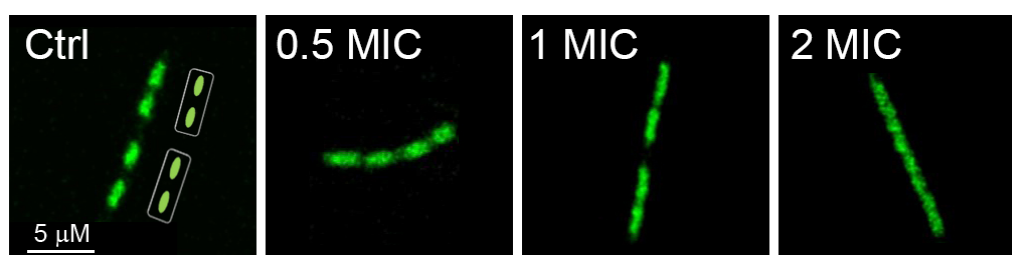
Fig. 6. Confocal microscopy of *B. subtilis* with RNAP fluorescence where **8e** was added to the culture at 0.5, 1, and 2 MIC.

2.4.3. Quantification of major cellular macromolecules

Next, we measured levels of major macromolecules in *S. aureus* ATCC 29213 cells treated with **8e** and rifampicin, in comparison with a no-treatment control. **8e** and rifampicin were added to staphylococcal cells in liquid culture at ¼, and ⅛ MIC levels at the end of the lag phase ($OD_{600} = 0.2$), and cells were harvested during mid-log phase ($OD_{600} = 0.6$). Consistent with their effect on cellular transcription, total levels of DNA were largely unaffected by either **8e** or rifampicin, as compared to the untreated control (Fig. 7A). In contrast to a more conventional measurement of *de novo* RNA synthesis, the total RNA was measured in this case, reducing the apparent inhibition. Total RNA levels were significantly reduced following exposure to rifampicin, consistent with its known mechanism of action and previous observations [43]. Treatment with **8e** closely mirrored the inhibitory effects of rifampicin, reducing the total levels of staphylococcal RNA in a dose-dependent manner (Fig. 7B). Interestingly, and in contrast to rifampicin, **8e** also reduced the total levels of protein observed in *S. aureus* ATCC 29213 (Fig. 7C). We speculate that this difference could be explained by the difference in the mechanism of rifampicin and **8e**. Rifampicin binds to an internal site on the β subunit of RNAP and interferes with the nascent RNA chain extension [44]. By contrast, **8e** was designed to interact with the exposed β'CH region, which serves as a major binding site not only for σ but also for NusG, which is proposed to modulate translation [45]. A possibility that **8e** may also inhibit RNAP binding to NusG will be investigated in future studies.
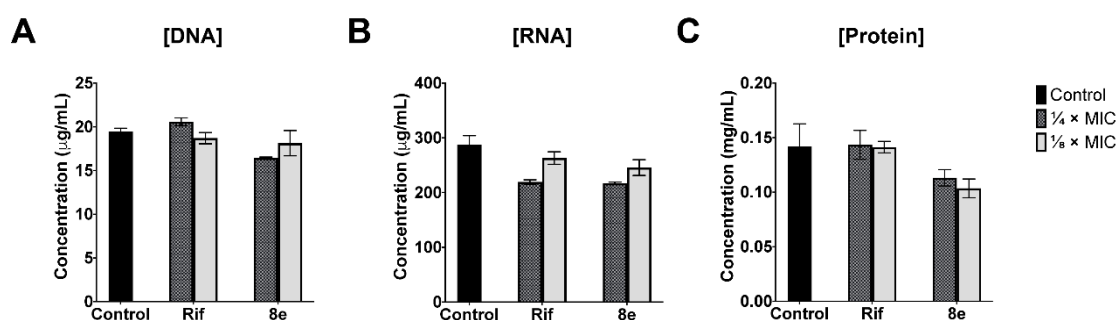
Fig. 7. The effects of **8e** on the levels of (**A**) DNA, (**B**) RNA and (**C**) protein of *S. aureus* ATCC 29213 when challenged at ¼ × (checkered bars) and ⅛ × (light grey bars) MICs compared to the control drug rifampicin (Rif) and the no-drug control (solid black bars).

Taking together, our observations that **8e** inhibited the β'CH-σ interaction *in vitro* (Fig. 5 & Table 2), altered subcellular localization of the transcription complex (Fig. 6), and suppressed RNA synthesis at the cellular level (Fig. 7), strongly suggest that the antimicrobial activities of **8e** resulted from the interference with bacterial transcription as designed.

2.5. Cytotoxicity

We evaluated the cytotoxicity of selected compounds **5b**, **5f**, **8e**, and **5e** against human HepG2 hepatocellular carcinoma and A549 lung carcinoma cell lines. All the tested compounds demonstrated very little cytotoxicity to these two human cancer cell lines, as compared with the cisplatin control (Table 3). This result indicates that our compounds have a potential for further development as novel antimicrobial agents.

Table 3. Cytotoxicity and therapeutic index of selected compounds

No.	CC_{50} (μM)		Therapeutic Index[a]	
	HepG2	A549	HepG2	A549
5b	$3.90 \times 10^3 \pm 2.83$	$2.40 \times 10^4 \pm 3.20$	1.82×10^3	1.12×10^4
5f	$3.41 \times 10^3 \pm 6.43$	$1.48 \times 10^4 \pm 7.49$	1.71×10^3	7.40×10^3

8e	387 ± 6.25	$1.84 \times 10^3 \pm 5.98$	199	946
5e	145 ± 7.87	129 ± 6.99	145	129
DDP[b]	4.35 ± 0.23	5.26 ± 0.32	-	-

[a] Calculated by CC_{50} / ½ MIC; [b] DDP: Cisplatin

2.6 Metabolic stability

To explore the feasibility for further development, metabolic stability was investigated using compound **8a**. Rat liver microsomes were employed with carbamazepine (CBZ) as the positive control according to the established method [46]. After microsomal incubation of **8a** at 10 μM and 50 μM, the average percentage of the remaining compound was maintained at 100%, whereas that of carbamazepine reduced to 45% (Table 4). The results indicated that **8a** was stable under the testing conditions and suggested its steady *in vivo* concentration with minimal metabolism.

Table 4. Metabolic stability of **8a** in rat liver microsomes

No.	% Metabolism	
	10 μM	50 μM
8a	98.28 ± 2.68	113.68 ± 13.06
CBZ	39.44 ± 3.32	48.86 ± 5.27

3. Conclusions

In this article, we report structural optimization, biological evaluation, and mechanistic validation of a bacterial transcription inhibitor targeting RNAP β'CH-σ binding

interface. A series of benzoyl and benzyl benzoic acid derivatives were synthesized based on a dichlorobenzyl lead compound, and their antibacterial activities against *S. pneumoniae* and *S. aureus* strains were used to evaluate important pharmacophores. The results showed that structural flexibility at the benzyl group did not affect the antibacterial activity and that the rigid benzoyl structure may present the active conformation for activity [47]. Substitution on the right benzene ring is important, as reflected by changes in both protein-binding inhibition and antibacterial activities. Electron-withdrawing and donating substituents can both improve the antibacterial activity, while electron-withdrawing groups were preferred, probably because of increased ionic bonding interaction between benzoic acid and β'CH residues R278 and R281, which are critical for σ binding. *Para*-substituted derivatives demonstrated greater activity than meta isomers.

The most potent trifluoromethyl derivative **8e** was chosen to test against a panel of clinically important Gram-positive pathogenic bacteria. The best result was obtained against *S. epidermidis,* with an MIC value of 0.5 μg/mL equal to that of vancomycin, the last-resort antibiotic in clinical practice. In addition, **8e** displayed antibacterial activity against *C. difficile*, including type strain and clinical isolates. *C. difficile,* an opportunistic pathogen causing fatal diarrhea and associated diseases, produces cytotoxins responsible for hypervirulence. **8e** inhibited toxin secretion of *C. difficile* at sub-MIC levels without affecting cell growth, similarly to fidaxomicin, another inhibitor of transcription that has been approved for treatment of *C. difficile* infections. antibiotic drug. The toxin secretion inhibitory effect of **8e** was even more significant compared to vancomycin as a common therapeutic choice in clinics for treating *C. difficile* infections [48].

Mechanistic studies were first carried out using *in vitro* protein complement assay. Several representative compounds were evaluated, and IC_{50} values of these compounds reached the sub-μM level, suggesting structural modifications maintained the protein-ligand affinity. When the experiment was carried out within the whole-cell system, fluorescence microscopy demonstrated representative compound **8e** started to disrupt the normal functions of RNAP and cause nucleoid delocalization in cells even at a sub-MIC level. Likewise, cell content quantification demonstrated that bacteria treated by sub-MIC of **8e** reduced RNA production as rifampicin, a transcription inhibitor antibiotic drug, while normal cell growth was maintained.

Finally, cytotoxicity measurement showed that these series of compounds exhibited exceptionally low toxic effects on two human cell lines, and rat liver microsomal metabolism assay demonstrated significant stability compared to carbamazepine. The experimental results suggest that these series of compounds are potential for further studies towards antibiotic development.

4. Experimental section

4.1. Chemistry

4.1.1. General methods

All reactions were monitored by thin-layer chromatography (TLC) on glass sheets (Silica gel F_{254}) which can be visualized under UV light. Flash chromatography was carried out using silica gel (200 – 300 mesh). Commercial reagents and anhydrous solvents were used without further purification. All yields reported were isolated yields. ^{1}H NMR (400 MHz) and ^{13}C NMR (100 MHz) spectra were generated from a BRUKER AVANCE-III spectrometer with TMS as an internal standard. Chemical shifts were

expressed in δ (ppm) and coupling constants (J) in Hz. High resolution MS spectra were measured using a Micromass® QTOF-2 spectrometer by electron spray ionization. HPLC analysis was performed on an Agilent 1260 HPLC apparatus.

*4.1.2. General procedure for the synthesis of intermediates **3a** – **j** (Scheme 1)*

To a Schlenk flask was added 4-(bromomethyl)-1-fluoro-2-nitrobenzene (234 mg, 1.0 mmol), an arylboronic acid from **2a** – **j** (1.2 mmol), Pd(OAc)$_2$ (12 mg, 0.05 mmol), PPh$_3$ (26 mg, 10%), K$_3$PO$_4$ (425 mg, 2.0 mmol) and toluene (10 ml) under nitrogen. After stirring at 80 °C for 12 h, the solvent was removed by evaporation and water was added. The mixture was extracted with DCM. The organic layer was concentrated and purified by silica gel column chromatography with hexane/ethyl acetate (15 : 1 to 10 : 1) as the eluent.

*4.1.3. Methyl 2-(4-fluoro-3-nitrobenzyl)benzoate (**3a**)*

Colorless oil (207 mg, 72%). ^{1}H NMR (400 MHz, CDCl$_3$) δ 7.98 (dd, J = 7.8, 1.2 Hz, 1H), 7.83 (dd, J = 7.1, 2.1 Hz, 1H), 7.51 (td, J = 7.6, 1.3 Hz, 1H), 7.43 (ddd, J = 6.7, 4.1, 2.2 Hz, 1H), 7.36 (td, J = 7.8, 1.1 Hz, 1H), 7.25 – 7.28 (m, 1H), 7.16 (dd, J = 10.6, 8.7 Hz, 1H), 4.42 (s, 2H), 3.84 (s, 3H).

*4.1.4. Methyl 4-chloro-2-(4-fluoro-3-nitrobenzyl)benzoate (**3b**)*

Colorless oil (173 mg, 56%). ^{1}H NMR (400 MHz, CDCl$_3$) δ 7.94 (d, J = 8.4 Hz, 1H), 7.84 (dd, J = 7.0, 2.1 Hz, 1H), 7.43 (ddd, J = 8.3, 4.1, 2.4 Hz, 1H), 7.34 (dd, J = 8.4, 2.0 Hz, 1H), 7.28 – 7.15 (m, 2H), 4.40 (s, 2H), 3.84 (s, 3H).

*4.1.5. Methyl 5-chloro-2-(4-fluoro-3-nitrobenzyl)benzoate (**3c**)*

Colorless oil (200 mg, 62%). ^{1}H NMR (400 MHz, CDCl$_3$) δ 7.97 (d, J = 2.3 Hz, 1H), 7.81 (dd, J = 7.0, 2.1 Hz, 1H), 7.48 (dd, J = 8.2, 2.3 Hz, 1H), 7.41 (ddd, J = 8.5, 4.0, 2.4 Hz, 1H), 7.23 – 7.14 (m, 2H), 4.38 (s, 2H), 3.85 (s, 3H).

4.1.6. Methyl 2-(4-fluoro-3-nitrobenzyl)-4-methoxybenzoate (3d)

White solid (220 mg, 69%). ^{1}H NMR (400 MHz, CDCl$_3$) δ 8.02 (d, J = 8.8 Hz, 1H), 7.82 (dd, J = 7.1, 2.1 Hz, 1H), 7.44 (ddd, J = 8.2, 4.1, 2.4 Hz, 1H), 7.16 (dd, J = 10.4, 8.8 Hz, 1H), 6.84 (dd, J = 8.8, 2.5 Hz, 1H), 6.74 (d, J = 2.6 Hz, 1H), 4.42 (s, 2H), 3.85 (s, 3H), 3.80 (s, 3H).

4.1.7. Methyl 2-(4-fluoro-3-nitrobenzyl)-4-(trifluoromethyl)benzoate (3e)

Colorless oil (182 mg, 51%). ^{1}H NMR (400 MHz, CDCl$_3$) δ 8.08 (d, J = 8.2 Hz, 1H), 7.84 (dd, J = 7.0, 2.0 Hz, 1H), 7.63 (d, J = 8.2 Hz, 1H), 7.51 (s, 1H), 7.40 (ddd, J = 8.3, 3.9, 2.5 Hz, 1H), 7.20 (dd, J = 10.5, 8.7 Hz, 1H), 4.46 (s, 2H), 3.87 (s, 3H).

4.1.8. Methyl 2-(4-fluoro-3-nitrobenzyl)-5-(trifluoromethyl)benzoate (3f)

Colorless oil (210 mg, 64%). ^{1}H NMR (400 MHz, CDCl$_3$) δ 8.25 (s, 1H), 7.84 (dd, J = 7.0, 2.1 Hz, 1H), 7.75 (d, J = 8.0 Hz, 1H), 7.43 (ddd, J = 14.7, 8.1, 5.3 Hz, 2H), 7.20 (dd, J = 10.5, 8.6 Hz, 1H), 4.49 (s, 2H), 3.89 (s, 3H).

4.1.9. Methyl 4-fluoro-2-(4-fluoro-3-nitrobenzyl)benzoate (3g)

Colorless oil (200 mg, 72%). ^{1}H NMR (400 MHz, CDCl$_3$) δ 8.04 (dd, J = 8.7, 6.0 Hz, 1H), 7.84 (dd, J = 7.0, 2.1 Hz, 1H), 7.46 – 7.40 (m, 1H), 7.19 (dd, J = 10.5, 8.6 Hz, 1H), 7.05 (td, J = 8.4, 2.6 Hz, 1H), 6.93 (dd, J = 9.4, 2.6 Hz, 1H), 4.43 (s, 2H), 3.84 (s, 3H).

4.1.10. Methyl 3-(4-fluoro-3-nitrobenzyl)benzoate (3h)

Colorless oil (145 mg, 50%). ^{1}H NMR (400 MHz, CDCl$_3$) δ 7.94 (d, J = 7.6 Hz, 1H), 7.89 – 7.83 (m, 2H), 7.48 – 7.34 (m, 3H), 7.22 (dd, J = 10.5, 8.6 Hz, 1H), 4.08 (s, 2H), 3.91 (s, 3H).

4.1.11. Methyl 2-(4-fluoro-3-nitrobenzyl)-4-methylbenzoate (3i)

Colorless oil (130 mg, 45%). ^{1}H NMR (400 MHz, CDCl$_3$) δ 7.90 (d, J = 8.0 Hz, 1H), 7.82 (dd, J = 7.1, 2.1 Hz, 1H), 7.48 – 7.37 (m, 1H), 7.22 – 7.11 (m, 2H), 7.06 (s, 1H), 4.39 (s, 2H), 3.81 (d, J = 4.1 Hz, 3H), 2.39 (s, 3H).

4.1.12. 1-Fluoro-4-(2-methoxybenzyl)-2-nitrobenzene (3j)

Colorless oil (188 mg, 72%). ^{1}H NMR (400 MHz, CDCl$_3$) δ 7.90 (dd, J = 7.1, 2.0 Hz, 1H), 7.45 (ddd, J = 8.4, 4.2, 2.4 Hz, 1H), 7.25 (dd, J = 15.4, 1.6 Hz, 1H), 7.19 – 7.10 (m, 2H), 6.92 (t, J = 7.3 Hz, 1H), 6.88 (d, J = 8.2 Hz, 1H), 3.99 (s, 2H), 3.80 (s, 3H).

4.1.13. General procedure for the synthesis of intermediates 4a – i and 5j (Scheme 1)

To a flask was added a compound from **3a** – **j** (0.2 mmol), 3,4-dichlorobenzenethiol (31 μL, 0.24 mmol), NaOAc (82 mg, 1 mmol) and EtOH 5 ml. The mixture was heated to reflux for 4 h. After cooling to room temperature, the precipitate was collected *via* filtration and washed with appropriate amount of EtOH and water successively and dried *in vacuo* to give the titled compound. Otherwise, water was added and then the mixture was extracted with EtOAc. The combined organic layers were dried over Na$_2$SO$_4$, concentrated and purified by chromatography with hexane/ethyl acetate (10 : 1) as the eluent to provide the titled compound.

4.1.14. Methyl 2-(4-((3,4-dichlorophenyl)thio)-3-nitrobenzyl)benzoate (4a)

Yellow solid (50 mg, 56%). ^{1}H NMR (400 MHz, CDCl$_3$) δ 8.04 (d, J = 1.5 Hz, 1H), 7.98 (dd, J = 7.8, 0.9 Hz, 1H), 7.66 (d, J = 2.0 Hz, 1H), 7.53 (d, J = 8.2 Hz, 1H), 7.50

(dd, *J* = 7.6, 1.1 Hz, 1H), 7.37 (dd, *J* = 11.2, 5.0 Hz, 2H), 7.25 (dd, *J* = 14.0, 5.2 Hz, 2H), 6.79 (d, *J* = 8.4 Hz, 1H), 4.42 (s, 2H), 3.86 (s, 3H).

4.1.15. Methyl 4-chloro-2-(4-((3,4-dichlorophenyl)thio)-3-nitrobenzyl)benzoate (*4b*)

Yellow solid (66 mg, 68%). ^{1}H NMR (400 MHz, CDCl$_3$) δ 8.03 (d, *J* = 1.5 Hz, 1H), 7.92 (d, *J* = 8.5 Hz, 1H), 7.66 (d, *J* = 2.0 Hz, 1H), 7.52 (d, *J* = 8.2 Hz, 1H), 7.38 (dd, *J* = 8.3, 2.0 Hz, 1H), 7.32 (dd, *J* = 8.4, 2.0 Hz, 1H), 7.20 (dd, *J* = 8.8, 1.8 Hz, 2H), 6.78 (d, *J* = 8.4 Hz, 1H), 4.38 (s, 2H), 3.84 (s, 3H).

4.1.16. Methyl 5-chloro-2-(4-((3,4-dichlorophenyl)thio)-3-nitrobenzyl)benzoate (*4c*)

Yellow solid (70 mg, 72%). ^{1}H NMR (400 MHz, CDCl$_3$) δ 8.00 (d, *J* = 1.5 Hz, 1H), 7.95 (d, *J* = 2.2 Hz, 1H), 7.64 (d, *J* = 2.0 Hz, 1H), 7.52 (d, *J* = 8.3 Hz, 1H), 7.45 (dd, *J* = 8.2, 2.3 Hz, 1H), 7.37 (dd, *J* = 8.3, 2.0 Hz, 1H), 7.22 – 7.14 (m, 2H), 6.77 (d, *J* = 8.4 Hz, 1H), 4.36 (s, 2H), 3.85 (s, 3H).

4.1.17. Methyl 2-(4-((3,4-dichlorophenyl)thio)-3-nitrobenzyl)-4-methoxybenzoate (*4d*)

Yellow solid (73 mg, 76%). ^{1}H NMR (400 MHz, CDCl$_3$) δ 8.01 (d, *J* = 2.0 Hz 1H), 8.00 (d, *J* = 8.9 Hz, 1H), 7.65 (d, *J* = 1.9 Hz, 1H), 7.51 (d, *J* = 8.3 Hz, 1H), 7.37 (dd, *J* = 8.3, 1.9 Hz, 1H), 7.23 (dd, *J* = 8.4, 1.6 Hz, 1H), 6.82 (dd, *J* = 8.8, 2.6 Hz, 1H), 6.77 (d, *J* = 8.4 Hz, 1H), 6.72 (d, *J* = 2.5 Hz, 1H), 4.40 (s, 2H), 3.84 (s, 3H), 3.80 (s, 3H).

4.1.18. Methyl 2-(4-((3,4-dichlorophenyl)thio)-3-nitrobenzyl)-4-(trifluoromethyl)benzoate (*4e*)

Yellow solid (58 mg, 57%). ^{1}H NMR (400 MHz, CDCl$_3$) δ 8.08 (d, *J* = 8.3 Hz, 1H), 8.06 (d, *J* = 1.5 Hz, 1H), 7.68 (d, *J* = 2.0 Hz, 1H), 7.62 (d, *J* = 8.7 Hz, 1H), 7.54 (d, *J* = 8.3 Hz, 1H), 7.52 (s, 1H), 7.38 – 7.42 (m, 1H), 7.19 (dd, *J* = 8.4, 1.8 Hz, 1H), 6.80 (d, *J* = 8.4 Hz, 1H), 4.45 (s, 2H), 3.89 (s, 3H).

4.1.19.   Methyl   2-(4-((3,4-dichlorophenyl)thio)-3-nitrobenzyl)-5-(trifluoromethyl)benzoate (4f)

Yellow solid (64 mg, 62%). ^{1}H NMR (400 MHz, CDCl$_3$) δ 8.23 (s, 1H), 8.03 (s, 1H), 7.72 (d, *J* = 8.3 Hz, 1H), 7.65 (d, *J* = 2.0 Hz, 1H), 7.56 (d, *J* = 2.1 Hz, 2H), 7.52 (d, *J* = 8.3 Hz, 1H), 7.20 (dd, *J* = 8.5, 1.8 Hz, 1H), 6.78 (d, *J* = 8.4 Hz, 1H), 4.46 (s, 2H), 3.88 (s, 3H).

4.1.20. Methyl 2-(4-((3,4-dichlorophenyl)thio)-3-nitrobenzyl)-4-fluorobenzoate (4g)

Yellow solid (61 mg, 65%). ^{1}H NMR (400 MHz, CDCl$_3$) δ 8.02 (dd, *J* = 8.7, 6.0 Hz, 2H), 7.66 (d, *J* = 2.0 Hz, 1H), 7.52 (d, *J* = 8.3 Hz, 1H), 7.38 (dd, *J* = 8.2, 2.0 Hz, 1H), 7.21 (dd, *J* = 8.5, 1.8 Hz, 1H), 7.06 – 6.98 (m, 1H), 6.91 (dd, *J* = 9.4, 2.5 Hz, 1H), 6.79 (d, *J* = 8.4 Hz, 1H), 4.40 (s, 2H), 3.84 (s, 3H).

4.1.21. Methyl 3-(4-((3,4-dichlorophenyl)thio)-3-nitrobenzyl)benzoate (4h)

Yellow solid (63 mg, 70%). ^{1}H NMR (400 MHz, CDCl$_3$) δ 8.06 (d, *J* = 1.6 Hz, 1H), 7.91 (s, 1H), 7.85 (s, 1H), 7.66 (d, *J* = 1.9 Hz, 1H), 7.53 (d, *J* = 8.2 Hz, 1H), 7.41 – 7.34 (m, 3H), 7.21 (dd, *J* = 8.3, 1.8 Hz, 1H), 6.80 (d, *J* = 8.4 Hz, 1H), 4.04 (s, 2H), 3.91 (s, 3H).

4.1.22. Methyl 2-(4-((3,4-dichlorophenyl)thio)-3-nitrobenzyl)-4-methylbenzoate (4i)

Yellow solid (67 mg, 72%). ^{1}H NMR (400 MHz, CDCl$_3$) δ 8.01 (d, *J* = 1.3 Hz, 1H), 7.88 (d, *J* = 8.0 Hz, 1H), 7.64 (d, *J* = 1.9 Hz, 1H), 7.51 (d, *J* = 8.3 Hz, 1H), 7.39 (dd, *J* = 9.9, 1.9 Hz, 1H), 7.35 (dd, *J* = 5.7, 1.9 Hz, 1H), 7.22 (dd, *J* = 8.5, 1.6 Hz, 1H), 7.14 (d, *J* = 7.9 Hz, 1H), 6.76 (d, *J* = 8.4 Hz, 1H), 4.36 (s, 2H), 3.81 (s, 3H), 2.37 (s, 3H).

4.1.23. General procedure for the synthesis of intermediates 5a – i (Scheme 1)

The methyl ester of the title compound (0.1 mmol) was hydrolyzed with 1 M NaOH (0.5 mmol) in dioxane and H_2O (v/v = 1 : 1) at 50 °C overnight. The mixture was then diluted with a small amount of water and washed twice with DCM. The aqueous solution was acidified by addition of 2 M HCl. The precipitate was collected by filtration and washed with water to afford the title compound. If the compound was not pure at this stage of the procedure, it was purified by column chromatography with DCM/MeOH (25 : 1) as the eluent.

4.1.24. 2-(4-((3,4-Dichlorophenyl)thio)-3-nitrobenzyl)benzoic acid (5a)

Yellow solid (30 mg, 70%); mp 118 – 120 °C; ^{1}H NMR (400 MHz, DMSO-d_6) δ 8.12 (s, 1H), 7.87 (d, J = 1.4 Hz, 1H), 7.73 (dd, J = 11.5, 8.3 Hz, 2H), 7.52 (dd, J = 11.0, 4.6 Hz, 2H), 7.29 (t, J = 7.1 Hz, 1H), 7.21 (dd, J = 6.6, 3.4 Hz, 2H), 6.89 (d, J = 8.3 Hz, 1H), 4.41 (s, 2H). ^{13}C NMR (100 MHz, DMSO-d_6) δ 171.1, 145.8, 142.3, 139.0, 137.4, 136.4, 135.7, 135.2, 133.4, 133.0, 132.6, 132.5, 131.1, 130.3, 129.89, 129.85, 129.6, 126.6, 125.9, 37.9. HRMS (ESI): calcd for $C_{20}H_{12}Cl_2NO_4S$, [M-H]$^-$ 431.9870, found 431.9879. HPLC purity: 96.90%.

4.1.25. 4-Chloro-2-(4-((3,4-dichlorophenyl)thio)-3-nitrobenzyl)benzoic acid (5b)

Yellow solid (26 mg, 56%); mp 243 – 245 °C; ^{1}H NMR (400 MHz, DMSO-d_6) δ 8.18 (s, 1H), 7.89 (d, J = 1.8 Hz, 1H), 7.75 (d, J = 8.3 Hz, 1H), 7.70 (d, J = 8.3 Hz, 1H), 7.53 (dd, J = 8.3, 1.5 Hz, 2H), 7.29 (s, 1H), 7.24 (dd, J = 8.3, 1.6 Hz, 1H), 6.91 (d, J = 8.3 Hz, 1H), 4.43 (s, 2H). ^{13}C NMR (100 MHz, DMSO-d_6) δ 169.9, 145.8, 141.7, 141.4, 136.5, 135.7, 135.3, 133.7, 133.4, 133.0, 132.9, 132.6, 132.5, 132.2, 130.4, 129.6, 126.4, 126.0, 37.4. HRMS (ESI): calcd for $C_{20}H_{11}Cl_3NO_4S$, [M-H]$^-$ 465.9480, found 465.9486. HPLC purity: 99.68%.

4.1.26. 5-Chloro-2-(4-((3,4-dichlorophenyl)thio)-3-nitrobenzyl)benzoic acid (5c)

Yellow solid (19 mg, 40%); mp 186 – 188 °C; ^{1}H NMR (400 MHz, DMSO-d_6) δ 14.91 – 12.01 (br, 1H), 8.06 (s, 1H), 7.88 (s, 1H), 7.82 (s, 1H), 7.76 (d, J = 8.1 Hz, 1H), 7.55 (t, J = 7.6 Hz, 2H), 7.39 (t, J = 7.3 Hz, 2H), 6.92 (d, J = 8.2 Hz, 1H), 4.39 (s, 2H). ^{13}C NMR (100 MHz, DMSO-d_6) δ 168.0, 145.7, 140.7, 139.4, 136.6, 135.44, 135.36, 133.9, 133.7, 133.5, 133.4, 133.0, 132.6, 132.3, 132.0, 131.8, 130.4, 129.7, 125.8, 37.2. HRMS (ESI): calcd for $C_{20}H_{11}Cl_3NO_4S$, [M-H]$^-$ 465.9480, found 465.9486. HPLC purity: 100.00%.

*4.1.27. 2-(4-((3,4-Dichlorophenyl)thio)-3-nitrobenzyl)-4-methoxybenzoic acid (**5d**)*

Yellow solid (23 mg, 50%); mp 196 – 198 °C; ^{1}H NMR (400 MHz, CDCl$_3$) δ 8.10 (d, J = 8.8 Hz, 1H), 8.04 (s, 1H), 7.64 (d, J = 1.9 Hz, 1H), 7.50 (d, J = 8.3 Hz, 1H), 7.36 (dd, J = 8.3, 1.9 Hz, 1H), 7.20 (d, J = 8.2 Hz, 1H), 6.85 (dd, J = 8.8, 2.2 Hz, 1H), 6.76 (d, J = 8.4 Hz, 1H), 6.73 (d, J = 2.2 Hz, 1H), 4.42 (s, 2H), 3.85 (s, 3H). ^{13}C NMR (100 MHz, CDCl$_3$) δ 171.0, 163.4, 145.3, 144.2, 139.5, 136.9, 134.9, 134.64, 134.59, 134.5, 134.3, 133.9, 131.7, 128.4, 125.8, 120.1, 118.0, 111.7, 55.5, 39.1. HRMS (ESI): calcd for $C_{21}H_{14}Cl_2NO_5S$, [M-H]$^-$ 461.9975, found 461.9976. HPLC purity: 97.38%.

*4.1.28. 2-(4-((3,4-Dichlorophenyl)thio)-3-nitrobenzyl)-4-(trifluoromethyl)benzoic acid (**5e**)*

Yellow solid (31 mg, 60%); mp 79 – 81 °C; ^{1}H NMR (400 MHz, DMSO-d_6) δ 13.61 (s, 1H), 8.10 (d, J = 0.8 Hz, 1H), 8.01 (d, J = 8.1 Hz, 1H), 7.88 (d, J = 1.8 Hz, 1H), 7.82 (s, 1H), 7.74 (dd, J = 12.9, 8.3 Hz, 2H), 7.54 (dd, J = 8.3, 1.9 Hz, 1H), 7.40 (dd, J = 8.3, 1.2 Hz, 1H), 6.93 (d, J = 8.4 Hz, 1H), 4.48 (s, 2H). ^{13}C NMR (100 MHz, DMSO-d_6) δ 168.2, 145.6, 141.6, 140.2, 136.6, 135.62, 135.44, 135.43, 133.7, 133.6, 133.0, 132.6, 132.2, 131.2 (q, J = 31.7 Hz), 131.8, 129.7, 128.6 (d, J = 3.5 Hz), 125.9, 124.2 (d, J =

3.6 Hz), 124.1 (q, J = 271.1 Hz), 37.5. HRMS (ESI): calcd for $C_{21}H_{11}Cl_2F_3NO_4S$, [M-H]$^-$ 499.9743, found 499.9741. HPLC purity: 100.00%.

4.1.29. 2-(4-((3,4-Dichlorophenyl)thio)-3-nitrobenzyl)-5-(trifluoromethyl)benzoic acid (5f)

Yellow solid (33 mg, 65%); mp 167 – 169 °C; ^{1}H NMR (400 MHz, DMSO-d_6) δ 13.64 (s, 1H), 8.11 (s, 2H), 7.83 – 7.95 (m, 2H), 7.76 (d, J = 8.2 Hz, 1H), 7.57 (dd, J = 24.6, 7.7 Hz, 2H), 7.41 (d, J = 8.0 Hz, 1H), 6.93 (d, J = 8.3 Hz, 1H), 4.50 (s, 2H). ^{13}C NMR (100 MHz, DMSO-d_6) δ 167.8, 145.7, 145.3, 140.0, 136.6, 135.5, 135.4, 133.7, 133.6, 133.3, 133.0, 132.6, 132.4, 132.2, 129.7, 128.8 (d, J = 3.1 Hz), 128.0 (d, J = 32.4 Hz), 127.5 (d, J = 3.7 Hz), 126.0, 124.2 (q, J = 270.5 Hz), 37.6. HRMS (ESI): calcd for $C_{21}H_{11}Cl_2F_3NO_4S$, [M-H]$^-$ 499.9743, found 499.9751. HPLC purity: 99.80%.

4.1.30. 2-(4-((3,4-Dichlorophenyl)thio)-3-nitrobenzyl)-4-fluorobenzoic acid (5g)

Yellow solid (22 mg, 49%); mp 97 – 99 °C; ^{1}H NMR (400 MHz, DMSO-d_6) δ 8.13 (s, 1H), 7.95 – 7.83 (m, 2H), 7.76 (d, J = 8.3 Hz, 1H), 7.54 (d, J = 6.9 Hz, 1H), 7.49 (d, J = 8.1 Hz, 1H), 7.15 (d, J = 9.9 Hz, 1H), 7.10 (t, J = 8.5 Hz, 1H), 6.91 (d, J = 8.3 Hz, 1H), 4.45 (s, 2H). ^{13}C NMR (100 MHz, DMSO-d_6) δ 169.4, 163.4 (d, J = 248.5 Hz), 145.8, 143.3 (d, J = 8.3 Hz), 141.1, 136.5, 135.6, 135.3, 133.6, 133.5, 133.2, 133.0, 132.6, 132.4, 129.6, 125.9, 117.9 (d, J = 21.1 Hz), 113.7 (d, J = 20.8 Hz), 37.67. HRMS (ESI): calcd for $C_{20}H_{11}Cl_2FNO_4S$, [M-H]$^-$ 449.9775, found 449.9782. HPLC purity: 99.75%.

4.1.31. 3-(4-((3,4-Dichlorophenyl)thio)-3-nitrobenzyl)benzoic acid (5h)

Yellow solid (35 mg, 80%); mp 161 – 163 °C; ^{1}H NMR (400 MHz, DMSO-d_6) δ 8.13 (s, 1H), 7.91 (s, 1H), 7.79 (s, 1H), 7.76 (d, J = 8.1 Hz, 2H), 7.55 (d, J = 8.0 Hz, 1H), 7.49 (d, J = 8.2 Hz, 1H), 7.37 – 7.25 (m, 2H), 6.95 (d, J = 8.3 Hz, 1H), 4.06 (s, 2H). ^{13}C

NMR (100 MHz, DMSO-d_6) δ 169.9, 145.9, 141.2, 139.8, 137.2, 136.5, 135.6, 135.4, 133.5, 133.0, 132.6, 132.4, 131.4, 129.99, 129.96, 128.5, 127.8, 125.8, 39.9. HRMS (ESI): calcd for $C_{20}H_{12}Cl_2NO_4S$, [M-H]$^-$ 431.9870, found 431.9869. HPLC purity: 99.80%.

4.1.32. 2-(4-((3,4-Dichlorophenyl)thio)-3-nitrobenzyl)-4-methylbenzoic acid (5i)

Yellow solid (20 mg, 45%); mp 182 – 184 °C; ^{1}H NMR (400 MHz, DMSO-d_6) δ 12.82 (s, 1H), 8.04 (d, J = 1.2 Hz, 1H), 7.90 (s, 1H), 7.78 (dd, J = 11.3, 8.1 Hz, 2H), 7.54 (dd, J = 8.3, 1.8 Hz, 1H), 7.40 (dd, J = 8.3, 1.3 Hz, 1H), 7.24 – 7.13 (m, 2H), 6.92 (d, J = 8.4 Hz, 1H), 4.39 (s, 2H), 2.32 (s, 3H). ^{13}C NMR (100 MHz, DMSO-d_6) δ 168.8, 145.6, 142.8, 141.2, 141.0, 136.6, 135.44, 135.38, 133.5, 133.2, 133.0, 132.9, 132.6, 132.3, 131.5, 129.6, 128.0, 127.7, 125.7, 37.9, 21.4. HRMS (ESI): calcd for $C_{21}H_{14}Cl_2NO_4S$, [M-H]$^-$ 446.0026, found 446.0018. HPLC purity: 99.20%.

4.1.33. (3,4-Dichlorophenyl)(4-(2-methoxybenzyl)-2-nitrophenyl)sulfane (5j)

Yellow solid (23 mg, 66%); mp 105 – 107 °C; ^{1}H NMR (400 MHz, CDCl$_3$) δ 8.11 (s, 1H), 7.66 (d, J = 1.6 Hz, 1H), 7.53 (d, J = 8.3 Hz, 1H), 7.39 (dd, J = 8.2, 1.7 Hz, 1H), 7.32 – 7.22 (m, 2H), 7.13 (d, J = 7.2 Hz, 1H), 6.91 (dd, J = 16.1, 8.0 Hz, 2H), 6.80 (d, J = 8.4 Hz, 1H), 3.99 (s, 2H), 3.82 (s, 3H). ^{13}C NMR (100 MHz, CDCl$_3$) δ 157.2, 145.4, 140.0, 136.8, 134.5, 134.44, 134.43, 134.2, 133.9, 131.9, 131.7, 130.3, 128.5, 128.3, 127.7, 125.8, 120.7, 110.7, 55.3, 35.3. HRMS (ESI): calcd for $C_{20}H_{14}Cl_2NO_3S$, [M-H]$^-$ 418.0077, found 418.0059. HPLC purity: 98.67%.

4.1.34. General procedure for the synthesis of intermediates 6a – h (Scheme 2)

In a sealed tube, a compound from **3a – h** or **3j** (0.5 mmol), NBS (445 mg, 2.5 mmol) and water (45 μL, 2.5 mmol) were added CHCl$_3$ (2.0 mL). After heating at 65 – 85 °C for 12 h, the reaction mixture was quenched with Na$_2$S$_2$O$_3$ aqueous solution. The

mixture was extracted with DCM, washed by brine, dried over Na$_2$SO$_4$ and concentrated. The titled compounds were purified by chromatography with hexane/ethyl acetate (15 : 1 to 8 : 1) as the eluent.

4.1.35. Methyl 2-(4-fluoro-3-nitrobenzoyl)benzoate (6a)

White solid (81 mg, 53%). ^{1}H NMR (400 MHz, CDCl$_3$) δ 8.37 (dd, J = 7.1, 2.1 Hz, 1H), 8.12 (d, J = 8.2 Hz, 1H), 8.10 – 8.07 (m, 1H), 7.71 (td, J = 7.5, 1.1 Hz, 1H), 7.64 (td, J = 7.6, 1.1 Hz, 1H), 7.42 – 7.35 (m, 2H), 3.75 (s, 3H).

4.1.36. Methyl 4-chloro-2-(4-fluoro-3-nitrobenzoyl)benzoate (6b)

White solid (76 mg, 45%). ^{1}H NMR (400 MHz, CDCl$_3$) δ 8.36 (dd, J = 7.1, 2.1 Hz, 1H), 8.16 – 8.02 (m, 2H), 7.61 (dd, J = 8.4, 2.0 Hz, 1H), 7.46 – 7.32 (m, 2H), 3.74 (s, 3H).

4.1.37. Methyl 5-chloro-2-(4-fluoro-3-nitrobenzoyl)benzoate (6c)

Colorless jelly (126 mg, 74%). ^{1}H NMR (400 MHz, CDCl$_3$) δ 8.35 (dd, J = 7.1, 2.1 Hz, 1H), 8.09 (d, J = 1.9 Hz, 1H), 8.08 – 8.04 (m, 1H), 7.68 (dd, J = 8.2, 2.0 Hz, 1H), 7.39 (dd, J = 9.8, 8.9 Hz, 1H), 7.34 (d, J = 8.2 Hz, 1H), 3.76 (s, 3H).

4.1.38. Methyl 2-(4-fluoro-3-nitrobenzoyl)-4-methoxybenzoate (6d)

Colorless oil (93 mg, 56%). ^{1}H NMR (400 MHz, CDCl$_3$) δ 8.36 (dd, J = 7.1, 2.2 Hz, 1H), 8.13 – 8.03 (m, 2H), 7.37 (dd, J = 10.0, 8.8 Hz, 1H), 7.08 (dd, J = 8.8, 2.5 Hz, 1H), 6.83 (d, J = 2.5 Hz, 1H), 3.90 (s, 3H), 3.70 (s, 3H).

4.1.39. Methyl 2-(4-fluoro-3-nitrobenzoyl)-4-(trifluoromethyl)benzoate (6e)

Colorless jelly (160 mg, 86%). ^{1}H NMR (400 MHz, CDCl$_3$) δ 8.37 (dd, J = 7.0, 2.2 Hz, 1H), 8.25 (d, J = 8.2 Hz, 1H), 8.06 (ddd, J = 8.7, 4.2, 2.3 Hz, 1H), 7.91 (d, J = 7.5 Hz, 1H), 7.65 (s, 1H), 7.42 (dd, J = 9.8, 8.9 Hz, 1H), 3.78 (s, 3H).

4.1.40. Methyl 2-(4-fluoro-3-nitrobenzoyl)-5-(trifluoromethyl)benzoate (6f)

Colorless oil (102 mg, 55%). ^{1}H NMR (400 MHz, CDCl$_3$) δ 8.39 (s, 1H), 8.36 (dd, J = 7.1, 2.2 Hz, 1H), 8.07 (ddd, J = 8.6, 4.1, 2.2 Hz, 1H), 7.97 (d, J = 7.9 Hz, 1H), 7.52 (d, J = 7.9 Hz, 1H), 7.41 (dd, J = 9.8, 8.9 Hz, 1H), 3.81 (s, 3H).

4.1.41. Methyl 4-fluoro-2-(4-fluoro-3-nitrobenzoyl)benzoate (6g)

Colorless oil (80 mg, 50%). ^{1}H NMR (400 MHz, CDCl$_3$) δ 8.36 (dd, J = 7.1, 2.2 Hz, 1H), 8.16 (dd, J = 8.7, 5.3 Hz, 1H), 8.08 (ddd, J = 8.6, 4.1, 2.2 Hz, 1H), 7.40 (dd, J = 9.9, 8.9 Hz, 1H), 7.31 (td, J = 8.4, 2.5 Hz, 1H), 7.08 (dd, J = 8.0, 2.5 Hz, 1H), 3.74 (s, 3H).

4.1.42. Methyl 3-(4-fluoro-3-nitrobenzoyl)benzoate (6h)

Colorless oil (45 mg, 60%). ^{1}H NMR (400 MHz, CDCl$_3$) δ 8.51 (dd, J = 7.1, 2.1 Hz, 1H), 8.40 (s, 1H), 8.33 (d, J = 7.8 Hz, 1H), 8.12 (ddd, J = 8.5, 4.0, 2.2 Hz, 1H), 7.99 (d, J = 7.7 Hz, 1H), 7.65 (t, J = 7.8 Hz, 1H), 7.47 (dd, J = 10.0, 8.8 Hz, 1H), 3.96 (s, 3H).

4.1.43. (4-Fluoro-3-nitrophenyl)(2-methoxyphenyl)methanone (6i)

Colorless oil (106 mg, 77%). ^{1}H NMR (400 MHz, CDCl$_3$) δ 8.43 (dd, J = 7.1, 2.0 Hz, 1H), 8.09 (ddd, J = 8.5, 4.0, 2.1 Hz, 1H), 7.64 (dd, J = 8.8, 2.4 Hz, 1H), 7.55 (d, J = 2.4 Hz, 1H), 7.42 – 7.33 (m, 1H), 6.92 (d, J = 8.9 Hz, 1H), 3.71 (s, 3H).

4.1.44. General procedure for the synthesis of intermediates 7a – 7h (Scheme 2)

To a flask was added a compound from **6a – h** (0.2 mmol), 3,4-dichlorobenzenethiol (31 μL, 0.24 mmol), NaOAc (82 mg, 1 mmol) and EtOH (5 ml). The mixture was heated to reflux for 4 h. After cooling to room temperature, the precipitate was collected *via* filtration and washed with appropriate amount of EtOH and water successively and dried *in vacuo* to give the titled compound. Otherwise, water was added and then the

mixture was extracted with EtOAc. The combined organic layers were dried over Na$_2$SO$_4$, concentrated, and purified by chromatography with hexane/ethyl acetate (10 : 1 to 8 : 1) as the eluent to provide the titled compound.

*4.1.45. Methyl 2-(4-((3,4-dichlorophenyl)thio)-3-nitrobenzoyl)benzoate (**7a**)*

Yellow solid, 85 mg, 92% yield. ^{1}H NMR (400 MHz, CDCl$_3$) δ 8.55 (d, J = 1.6 Hz, 1H), 8.11 (d, J = 7.8 Hz, 1H), 7.82 (dd, J = 8.6, 1.7 Hz, 1H), 7.72 (d, J = 1.9 Hz, 1H), 7.69 (d, J = 6.7 Hz, 1H), 7.64 (d, J = 7.7 Hz, 1H), 7.61 (d, J = 8.3 Hz, 1H), 7.45 (dd, J = 8.2, 1.9 Hz, 1H), 7.37 (d, J = 7.4 Hz, 1H), 6.95 (d, J = 8.5 Hz, 1H), 3.76 (s, 3H).

*4.1.46. Methyl 4-chloro-2-(4-((3,4-dichlorophenyl)thio)-3-nitrobenzoyl)benzoate (**7b**)*

Yellow solid (61mg, 62%). ^{1}H NMR (400 MHz, CDCl$_3$) δ 8.53 (d, J = 1.7 Hz, 1H), 8.04 (d, J = 8.4 Hz, 1H), 7.78 (dd, J = 8.6, 1.8 Hz, 1H), 7.70 (d, J = 1.9 Hz, 1H), 7.58 (dd, J = 12.4, 5.2 Hz, 2H), 7.43 (dd, J = 8.2, 2.0 Hz, 1H), 7.32 (d, J = 1.9 Hz, 1H), 6.93 (d, J = 8.5 Hz, 1H), 3.74 (s, 3H).

*4.1.47. Methyl 5-chloro-2-(4-((3,4-dichlorophenyl)thio)-3-nitrobenzoyl)benzoate (**7c**)*

Yellow solid (60 mg, 61%). ^{1}H NMR (400 MHz, CDCl$_3$) δ 8.50 (d, J = 1.8 Hz, 1H), 8.06 (d, J = 2.0 Hz, 1H), 7.78 (dd, J = 8.6, 1.9 Hz, 1H), 7.70 (d, J = 2.0 Hz, 1H), 7.64 (dd, J = 8.1, 2.1 Hz, 1H), 7.59 (d, J = 8.3 Hz, 1H), 7.42 (dd, J = 8.3, 2.0 Hz, 1H), 7.30 (d, J = 8.1 Hz, 1H), 6.93 (d, J = 8.6 Hz, 1H), 3.75 (s, 3H).

*4.1.48. Methyl 2-(4-((3,4-dichlorophenyl)thio)-3-nitrobenzoyl)-4-methoxybenzoate (**7d**)*

Yellow solid (65 mg, 66%). ^{1}H NMR (400 MHz, CDCl$_3$) δ 8.53 (d, J = 1.7 Hz, 1H), 8.04 (d, J = 8.8 Hz, 1H), 7.80 (dd, J = 8.5, 1.7 Hz, 1H), 7.70 (d, J = 1.9 Hz, 1H), 7.58 (d, J = 8.3 Hz, 1H), 7.42 (dd, J = 8.2, 1.9 Hz, 1H), 7.05 (dd, J = 8.8, 2.5 Hz, 1H), 6.92 (d, J = 8.6 Hz, 1H), 6.79 (d, J = 2.5 Hz, 1H), 3.88 (s, 3H), 3.70 (s, 3H).

4.1.49. Methyl 2-(4-((3,4-dichlorophenyl)thio)-3-nitrobenzoyl)-4-(trifluoromethyl)benzoate (7e)

Yellow solid (76 mg, 72%). ^{1}H NMR (400 MHz, CDCl$_3$) δ 8.54 (d, J = 1.9 Hz, 1H), 8.22 (d, J = 8.2 Hz, 1H), 7.88 (s, 1H), 7.75 (dd, J = 8.6, 1.7 Hz, 1H), 7.70 (d, J = 1.8 Hz, 1H), 7.59 (d, J = 8.2 Hz, 2H), 7.43 (dd, J = 8.2, 1.7 Hz, 1H), 6.94 (d, J = 8.5 Hz, 1H), 3.78 (s, 2H).

4.1.50. Methyl 2-(4-((3,4-dichlorophenyl)thio)-3-nitrobenzoyl)-5-(trifluoromethyl)benzoate (7f)

Yellow solid (73 mg, 69%). ^{1}H NMR (400 MHz, CDCl$_3$) δ 8.52 (d, J = 1.8 Hz, 1H), 8.37 (s, 1H), 7.94 (d, J = 7.8 Hz, 1H), 7.77 (dd, J = 8.6, 1.9 Hz, 1H), 7.70 (d, J = 2.0 Hz, 1H), 7.59 (d, J = 8.3 Hz, 1H), 7.48 (d, J = 7.9 Hz, 1H), 7.43 (dd, J = 8.3, 2.0 Hz, 1H), 6.94 (d, J = 8.6 Hz, 1H), 3.80 (s, 3H).

4.1.51. Methyl 2-(4-((3,4-dichlorophenyl)thio)-3-nitrobenzoyl)-4-fluorobenzoate (7g)

Yellow solid (68 mg, 71%). ^{1}H NMR (400 MHz, CDCl$_3$) δ 8.52 (d, J = 1.8 Hz, 1H), 8.13 (dd, J = 8.7, 5.3 Hz, 1H), 7.79 (dd, J = 8.6, 1.9 Hz, 1H), 7.70 (d, J = 2.0 Hz, 1H), 7.59 (d, J = 8.2 Hz, 1H), 7.43 (dd, J = 8.3, 2.0 Hz, 1H), 7.32 – 7.27 (m, 1H), 7.04 (dd, J = 8.0, 2.5 Hz, 1H), 6.94 (d, J = 8.6 Hz, 1H), 3.73 (s, 3H).

4.1.52. Methyl 3-(4-((3,4-dichlorophenyl)thio)-3-nitrobenzoyl)benzoate (7h)

Yellow solid (65 mg, 70%). ^{1}H NMR (400 MHz, CDCl$_3$) δ 8.67 (d, J = 1.8 Hz, 1H), 8.38 (s, 1H), 8.30 (d, J = 7.8 Hz, 1H), 7.97 (d, J = 7.8 Hz, 1H), 7.84 (dd, J = 8.5, 1.8 Hz, 1H), 7.74 (d, J = 2.0 Hz, 1H), 7.66 – 7.58 (m, 2H), 7.47 (dd, J = 8.2, 2.0 Hz, 1H), 7.00 (d, J = 8.5 Hz, 1H), 3.95 (s, 3H).

4.1.53. General procedure for the synthesis of compounds 8a – h (Scheme 2)

The methyl ester of the title compound was hydrolyzed with 1 M NaOH in dioxane and H$_2$O (v/v = 1 : 1) at 50 °C overnight. The mixture was then diluted with a small amount of water and washed twice with DCM. The aqueous solution was acidified by addition of 2 M HCl. The precipitate was collected by filtration and washed with water to afford the title compound. If the compound was not pure at this stage of the procedure, it was purified by silica gel column chromatography with DCM/MeOH (20 : 1) as the eluent.

4.1.54. 2-(4-((3,4-Dichlorophenyl)thio)-3-nitrobenzoyl)benzoic acid (8a)

Yellow solid, (58 mg, 62%); mp 246 – 248 °C; ^{1}H NMR (400 MHz, DMSO-d_6) δ 13.34 (s, 1H), 8.37 (s, 1H), 8.02 (d, *J* = 13.0 Hz, 2H), 7.84 (d, *J* = 8.3 Hz, 1H), 7.76 (dd, *J* = 14.9, 7.7 Hz, 2H), 7.72 – 7.67 (m, 1H), 7.64 (d, *J* = 8.0 Hz, 1H), 7.46 (d, *J* = 6.8 Hz, 1H), 7.07 (d, *J* = 8.4 Hz, 1H). ^{13}C NMR (100 MHz, DMSO-d_6) δ 194.4, 167.2, 144.8, 142.7, 140.7, 137.4, 136.1, 135.0, 134.4, 134.1, 133.3, 132.9, 130.8, 130.7, 130.5, 130.1, 129.5, 127.8, 125.8. HRMS (ESI): calcd for C$_{20}$H$_{10}$Cl$_2$NO$_5$S, [M-H]$^-$ 445.9662, found 445.9651. HPLC purity: 99.73%.

4.1.55. 4-Chloro-2-(4-((3,4-dichlorophenyl)thio)-3-nitrobenzoyl)benzoic acid (8b)

Yellow solid (27 mg, 55%); mp 229 – 231 °C; ^{1}H NMR (400 MHz, DMSO-d_6) δ 13.43 (s, 1H), 8.39 (d, *J* = 1.5 Hz, 1H), 8.05 – 7.92 (m, 2H), 7.84 (d, *J* = 8.3 Hz, 1H), 7.80 – 7.70 (m, 2H), 7.69 – 7.59 (m, 1H), 7.05 (d, *J* = 8.6 Hz, 1H). ^{13}C NMR (100 MHz, DMSO-d_6) δ 192.9, 166.4, 144.9, 142.8, 138.4, 137.4, 136.2, 134.7, 134.5, 134.2, 133.3, 132.9, 132.3, 130.70, 130.68, 129.5, 128.8, 127.6, 125.7, 120.2. HRMS (ESI): calcd for C$_{20}$H$_9$Cl$_3$NO$_5$S, [M-H]$^-$ 479.9272, found 479.9265. HPLC purity: 92.07%.

4.1.56. 5-Chloro-2-(4-((3,4-dichlorophenyl)thio)-3-nitrobenzoyl)benzoic acid (8c)

Yellow solid (26 mg, 58%); mp 246 – 248 °C; ^{1}H NMR (400 MHz, DMSO-d_6) δ 8.32 (d, *J* = 1.6 Hz, 1H), 7.99 (d, *J* = 1.6 Hz, 1H), 7.90 (d, *J* = 1.8 Hz, 1H), 7.82 (d, *J* = 8.3

Hz, 1H), 7.67 (d, J = 7.6 Hz, 2H), 7.63 (dd, J = 8.3, 1.9 Hz, 1H), 7.36 (d, J = 8.1 Hz, 1H), 7.01 (d, J = 8.5 Hz, 1H). ^{13}C NMR (100 MHz, DMSO-d_6) δ 192.8, 166.3, 144.8, 141.7, 139.3, 137.4, 136.1, 135.99, 135.97, 134.7, 134.3, 134.0, 133.3, 132.9, 131.2, 130.9, 129.6, 129.3, 129.0, 125.3. HRMS (ESI): calcd for $C_{20}H_9Cl_3NO_5S$, [M-H]$^-$ 479.9276, found 479.9272. HPLC purity: 96.70%.

*4.1.57. 2-(4-((3,4-Dichlorophenyl)thio)-3-nitrobenzoyl)-4-methoxybenzoic acid (**8d**)*

Yellow solid (19 mg, 40%); mp 218 – 220 °C; ^{1}H NMR (400 MHz, DMSO-d_6) δ 12.92 (s, 1H), 8.36 (s, 1H), 8.00 (d, J = 1.6 Hz, 1H), 7.96 (d, J = 8.7 Hz, 1H), 7.84 (d, J = 8.3 Hz, 1H), 7.72 (d, J = 8.5 Hz, 1H), 7.64 (dd, J = 8.3, 1.5 Hz, 1H), 7.18 (dd, J = 8.7, 2.2 Hz, 1H), 7.05 (d, J = 8.6 Hz, 1H), 6.97 (d, J = 2.1 Hz, 1H), 3.84 (s, 3H). ^{13}C NMR (100 MHz, DMSO-d_6) δ 194.0, 166.9, 163.0, 144.8, 143.5, 142.1, 137.4, 136.2, 135.4, 134.4, 134.0, 133.3, 132.9, 132.4, 130.8, 129.4, 125.5, 122.3, 115.7, 112.7, 56.3. HRMS (ESI): calcd for $C_{21}H_{12}Cl_2NO_6S$, [M-H]$^-$ 475.9768, found 475.9770. HPLC purity: 95.07%.

*4.1.58. 2-(4-((3,4-Dichlorophenyl)thio)-3-nitrobenzoyl)-4-(trifluoromethyl)benzoic acid (**8e**)*

Pale yellow solid (21 mg, 40%); mp 154 – 156 °C; ^{1}H NMR (400 MHz, DMSO-d_6) δ 8.35 (d, J = 1.5 Hz, 1H), 8.11 (d, J = 8.1 Hz, 1H), 7.98 (d, J = 1.9 Hz, 1H), 7.91 (d, J = 7.9 Hz, 1H), 7.82 (d, J = 8.3 Hz, 1H), 7.67 (s, 1H), 7.63 (ddd, J = 8.2, 4.4, 1.9 Hz, 2H), 7.01 (d, J = 8.6 Hz, 1H). ^{13}C NMR (100 MHz, DMSO-d_6) δ 192.8, 166.4, 144.8, 141.43, 141.36, 140.6, 137.4, 136.1, 134.3, 134.0, 133.3, 132.9, 131.1, 130.9, 130.8, 129.3, 126.7 (d, J = 3.3 Hz), 125.2, 124. 3 (q, J = 271 Hz), 123.8 (d, J = 3.4 Hz). HRMS (ESI): calcd for $C_{21}H_9Cl_2F_3NO_5S$, [M-H]$^-$ 513.9536, found 513.9529. HPLC purity: 95.40%.

*4.1.59. 2-(4-((3,4-Dichlorophenyl)thio)-3-nitrobenzoyl)-5-(trifluoromethyl)benzoic acid (**8f**)*

Yellow solid (18 mg, 35%); mp 181 – 183 °C; ^{1}H NMR (400 MHz, DMSO-d_6) δ 8.37 (d, J = 0.9 Hz, 1H), 8.21 (s, 1H), 7.99 (d, J = 1.8 Hz, 2H), 7.83 (d, J = 8.2 Hz, 1H), 7.64 (t, J = 7.5 Hz, 2H), 7.58 (d, J = 7.8 Hz, 1H), 7.01 (d, J = 8.5 Hz, 1H). ^{13}C NMR (100 MHz, DMSO-d_6) δ 195.0, 165.9, 144.9, 144.5, 141.9, 137.4, 136.1, 135.5, 134.4, 134.1, 133.3, 132.9, 130.8, 129.4, 129.2, 128.4, 128.3, 127.8, 126.6 (d, J = 3.3 Hz), 125.6, 125.2, 124.2 (q, J = 270.9 Hz). HRMS (ESI): calcd for $C_{21}H_9Cl_2F_3NO_5S$, [M-H]$^-$ 513.9516, found 513.9536. HPLC purity: 92.61%.

*4.1.60. 2-(4-((3,4-Dichlorophenyl)thio)-3-nitrobenzoyl)-4-fluorobenzoic acid (**8g**)*

Yellow solid (20 mg, 43%); mp 90 – 92 °C; ^{1}H NMR (400 MHz, DMSO-d_6) δ 13.29 (s, 1H), 8.37 (s, 1H), 8.06 (dd, J = 8.1, 5.6 Hz, 1H), 8.01 (s, 1H), 7.84 (d, J = 8.3 Hz, 1H), 7.72 (d, J = 8.3 Hz, 1H), 7.64 (d, J = 8.1 Hz, 1H), 7.49 (t, J = 7.5 Hz, 1H), 7.38 (d, J = 8.1 Hz, 1H), 7.04 (d, J = 8.5 Hz, 1H). ^{13}C NMR (100 MHz, DMSO-d_6) δ 166.4, 164.6 (d, J = 250.5 Hz), 144.9, 142.3, 137.4, 136.2, 135.1, 134.4, 134.1, 133.3, 132.9, 132.0, 130.8, 129.4, 129.2, 127.8, 125.5, 117.4 (d, J = 22.8 Hz), 114.8 (d, J = 24.0 Hz). HRMS (ESI): calcd for $C_{20}H_9Cl_2FNO_5S$, [M-H]$^-$ 463.9568, found 463.9570. HPLC purity: 97.19%.

*4.1.61. 3-(4-((3,4-Dichlorophenyl)thio)-3-nitrobenzoyl)benzoic acid (**8h**)*

Yellow solid (23 mg, 52%); mp 207 – 209 °C; ^{1}H NMR (400 MHz, DMSO-d_6) δ 8.52 (d, J = 1.6 Hz, 1H), 8.25 (s, 1H), 8.22 (d, J = 7.6 Hz, 1H), 8.05 (d, J = 1.9 Hz, 1H), 7.92 (dd, J = 8.5, 1.7 Hz, 1H), 7.90 – 7.82 (m, 2H), 7.70 (dd, J = 8.3, 1.9 Hz, 1H), 7.62 (t, J = 7.6 Hz, 1H), 7.14 (d, J = 8.5 Hz, 1H). ^{13}C NMR (100 MHz, DMSO-d_6) δ 193.3, 167.8, 144.7, 142.3, 137.4, 136.3, 136.2, 135.0, 134.8, 134.4, 134.1, 133.3, 132.9, 132.4, 130.8, 130.6, 129.3, 129.1, 127.3. HRMS (ESI): calcd for $C_{20}H_{10}Cl_2NO_5S$, [M-H]$^-$ 445.9666, found 445.9662. HPLC purity: 96.06%.

*4.1.62. (4-((3,4-Dichlorophenyl)thio)-3-nitrophenyl)(2-methoxyphenyl)methanone (**8i**)*

Yellow solid (34 mg, 77%); mp 139 – 141 °C; ^{1}H NMR (400 MHz, CDCl$_3$) δ 8.59 (d, J = 1.8 Hz, 1H), 7.81 (dd, J = 8.5, 1.8 Hz, 1H), 7.72 (d, J = 2.0 Hz, 1H), 7.64 – 7.57 (m, 2H), 7.49 (d, J = 2.5 Hz, 1H), 7.44 (dd, J = 8.3, 2.0 Hz, 1H), 7.26 (s, 1H), 6.91 (dd, J = 14.3, 8.7 Hz, 2H), 3.71 (s, 3H). ^{13}C NMR (100 MHz, CDCl$_3$) δ 191.6, 156.3, 144.6, 143.8, 137.2, 135.6, 135.5, 134.9, 134.7, 134.5, 133.5, 132.4, 132.2, 130.1, 129.0, 127.9, 127.4, 113.45, 113.38, 55.9. HRMS (ESI): calcd for C$_{20}$H$_{12}$Cl$_2$NO$_4$S, [M-H]$^-$ 431.9870, found 431.9873. HPLC purity: 95.41%.

4.2. Biology

4.2.1. Determination of minimum inhibitory concentration (MIC)

Antimicrobial activity of each compound was determined by broth microdilution according to the Clinical & Laboratory Standards Institute (CLSI) guidelines [49]. The test medium was cation-adjusted Mueller-Hinton Broth (MHB) for *Staphylococcus* spp. and Brain Heart Infusion (BHI) for *Streptococcus* spp. During screening, serial two-fold dilutions of the compound were performed starting from 256 µg/mL down to 0.5 µg/mL, and the bacterial inoculum calibrated to approximately 5×10^5 CFU/mL. Results were examined after incubation of 20 h at 37 °C, where the MIC was defined as the lowest concentration of antibiotic with no observable growth.

Three strains of *Clostridium difficile* were also used in this study, including the toxinotype 0 / ribotype 001 type strain *C. difficile* ATCC® 9689™ (positive for both TcdA and TcdB) and two clinical isolates ribotype 002 and ribotype 027. The test compound and control drugs vancomycin and fidaxomicin used in this work were first prepared as DMSO solutions and their MICs assessed anaerobically.

To remove dissolved oxygen, all media for *C. difficile* were incubated for 3 h in the anaerobic chamber prior to use. Colonies were first selected from overnight anaerobic culture on GAM agar before MIC assays were carried out in BHI supplemented with 0.5% w/v yeast extract and filter-sterilized 0.05% L-cysteine. *C. difficile* colonies in BHI were then allowed to grow anaerobically to early log phase before being diluted into a 0.5 McFarland suspension, which was further diluted by having 100 µL taken to inoculate 15 mL of BHI. 50 µL aliquots from this suspension were summarily used to inoculate wells pre-loaded with 50 µL BHI solutions containing serially diluted antimicrobial agents in 96-well plates. MIC plates were incubated at 37 °C and examined for growth at 48 h. Experiments were performed in triplicate.

4.2.2. Toxin secretion inhibition and CFU counting in C. difficile

C. difficile strains used in this section and their corresponding anaerobic culturing conditions were described above in Section 4.2.1. 120 µL of a 0.5 McFarland early log phase suspension of *C. difficile* was taken and further diluted into 18 mL of BHI. 300 µL aliquots from this *C. difficile* suspension were used to inoculate wells pre-loaded with 300 µL BHI solutions containing serially diluted antimicrobial agents in 48-well plates. Plates were then incubated anaerobically at 37 °C and samples were withdrawn at 48 h for total CFU counting on GAM agar using broth microdilution method. At 48 h, all cultures from wells ½, ¼, ⅛, 1/16 MICs, as well as the drug-free control, were harvested by centrifuging at 10,000 × *g* for 2 min and their supernatants retained for TcdA and TcdB toxin production by ELISA.

Quantification of TcdA and TcdB was performed with a commercial ELISA kit (Cat. No. TGC-E002-1, tgcBIOMICS GmbH, Germany) according to the manufacturer's instructions. Samples within each strain were diluted by the same factor to the range

recommended in the assay for better comparison across the ELISA results. All samples were tested in duplicate with technical and biological repeats.

4.2.3. Determination of inhibitory activity to β'CH-σ interaction

Inhibition assay was carried out following protein overproduction and purification based on previously established protocols [15]. 40 μL C-LgBiT-σ^A (0.125 μM in PBS) was added to 96-well plates loaded with 20 μL compound at desired concentrations. The mixture was incubated for 10 min at 37 °C, after which 40 μL C-SmBiT-CH (0.125 μM in PBS) was added to each well and a further 10 mins incubation period at 37 °C. Finally, 10 μL of 1:100 buffer-dissolved Promga NanoGlo® Luciferase Assay Substrate was added to the reaction mixture. Luminescence was measured using a Victor X3 Multilabel plate reader. The experiment was performed in triplicate with technical replicates.

4.2.4. Confocal fluorescence microscopy

B. subtilis strain BS1048 (RpoC-GFP) [14] was grown on LB agar plate. A single colony was incubated in LB medium supplemented at 37 °C until $OD_{600} \sim 0.6$. Compound at ¼ ½, 1, 2 MIC was then added to the culture and allowed to incubate for further 15 min. 2.5 μL of cell culture was placed onto 1.2% freshly made agarose plate and covered with a coverslip prior to imaging. Leica TCS SPE confocal microscope equipped with 63 × /1.3 oil objective and mercury metal halide bulb was used to capture the fluorescence images. The fluorescence images were processed with LAS X software.

4.2.5. Cell content quantification

The effects of varying concentrations of treatment compounds elicited on total levels of DNA, RNA and protein during cell growth was assessed by first preparing a master

culture of *S. aureus* ATCC 29213. First inoculated at OD_{600} 0.1 and agitated at 175 rpm at 37 °C, its confluence was doubled to 0.2 (early log phase) before being divided into aliquots where compounds and control drugs were added at their respective ¼ and ⅛ MICs, complete with a drug-free control culture. Cells were harvested upon the control reaching an OD_{600} of 0.6 (mid-log phase), where other samples were harvested at volumes adjusted to an OD_{600} equivalent of 0.6. 3 mL cultures were pelleted at 5000 × *g* for 5 min at 4 °C and the supernatant discarded. The major macromolecules were extracted and purified using the AllPrep® Bacterial DNA/RNA/Protein Kit (Qiagen) following the manufacturer's protocols, and the nucleic acid levels quantified with Qubit™ DNA BR Assay Kit (Invitrogen) and Qubit™ RNA BR Assay Kit (Invitrogen) in conjunction with a Qubit 4 Fluorometer (Thermo Fisher). Pierce BCA Protein Assay Kit (Thermo Fisher) was used to measure protein levels. The experiment was performed in triplicate.

4.2.6. Cytotoxicity assay

Human cell lines A549 lung carcinoma and HepG2 hepatocellular carcinoma were used in this study, where they were seeded at 2.5×10^5 cells per well and incubated for 24 hours at 37 °C. Test compounds were added in two-fold serial dilutions ranging from 50 μg/mL to 1.56 μg/mL. Plates were incubated for a further 24 h at 37 °C. MTT assay was performed at 48 h and 72 h post-addition of compounds as previously described [42]. 5-fluorouracil was used as the positive control and DMSO as the negative control.

4.2.7. Microsomal stability assay

Compound **8a** at 10 and 50 μM were pre-incubated with 1 mg/ml rat liver microsome and 6 mM $MgCl_2$ in 50 mM phosphate buffer (pH = 7.4) at 37 °C. The reaction was initiated by addition of 5 mM NADPH and terminated by adding 600 μl ice-cold

methanol after 60 min of incubation. After centrifugation of resulted reaction mixture at 12,000 × *g* for 10 min, the supernatant was obtained for analysis of the remaining concentrations of **8a** by LC/MS/MS method. The reaction system was validated using carbamazepine at 10 and 50 μM as positive controls as described [46] and the experiments were conducted in triplicates.

Appendix A. Supplementary data

Supplementary data to this article can be found online at https://

Abbreviations

MRSA methicillin-resistant Staphylococcus aureus

PPI protein-protein interaction

MIC minimum inhibition concentration

SAR structure-activity relationship

CD circular dichroism

QSAR quantitative structureeactivity relationship

rRNA ribosomal RNA

MIC minimum inhibition concentration

DCM dichloromethane

THF tetrahydrofuran

DMSO dimethyl sulfoxide

AcOH acetic acid

EtOAc ethyl acetate

References

[1] J. O'Neill, Antimicrobial Resistance: Tackling a Crisis for the Future Health and Wealth of Nations, Review on Antimicrobial Resistance, London, 2014.

[2] C. Ma, X. Yang, P.J. Lewis, Bacterial transcription as a target for antibacterial drug development, Microbiol. Mol. Biol. Rev. 80 (2016) 139–160.

[3] E.F. Ruff, M.T. Record, Jr., I. Artsimovitch, Initial events in bacterial transcription initiation, Biomolecules 5 (2015) 1035–1062.

[4] A. Feklistov, B.D. Sharon, S.A. Darst, C.A. Gross, Bacterial sigma factors: a historical, structural, and genomic perspective, Annu. Rev. Microbiol. 68 (2014) 357–376.

[5] S. Borukhov, E. Nudler, RNA polymerase holoenzyme: structure, function and biological implications, Curr. Opin. Microbiol. 6 (2003) 93–100.

[6] T.M. Gruber, D. Markov, M.M. Sharp, B.A. Young, C.Z. Lu, H.J. Zhong, I. Artsimovitch, K.M. Geszvain, T.M. Arthur, R.R. Burgess, R. Landick, K. Severinov, C.A. Gross, Binding of the initiation factor σ^{70} to core RNA polymerase is a multistep process, Mol. Cell 8 (2001) 21–31.

[7] R.R. Burgess, L. Anthony, How sigma docks to RNA polymerase and what sigma does, Curr. Opin. Microbiol. 4 (2001) 126–131.

[8] I. Artsimovitch, Post-initiation control by the initiation factor sigma, Mol. Microbiol. 68 (2008) 1–3.

[9] K.S. Murakami, S. Masuda, E.A. Campbell, O. Muzzin, S.A. Darst, Structural basis of transcription initiation: an RNA polymerase holoenzyme-DNA complex, Science 296 (2002) 1285–1290.

[10] B. Bae, A. Feklistov, A. Lass-Napiorkowska, R. Landick, S.A. Darst, Structure of a bacterial RNA polymerase holoenzyme open promoter complex, Elife 4 (2015) e08504.

[11] T.M. Arthur, R.R. Burgess, Localization of a σ^{70} binding site on the N terminus of the *Escherichia coli* RNA polymerase β' subunit, J. Biol. Chem. 273 (1998) 31381–31387.

[12] T.M. Arthur, L.C. Anthony, R.R. Burgess, Mutational analysis of $\beta'_{260-309}$, a σ^{70} binding site located on *Escherichia coli* core RNA polymerase, J. Biol. Chem. 275 (2000) 23113–23119.

[13] C. Ma, X. Yang, H. Kandemir, M. Mielczarek, E.B. Johnston, R. Griffith, N. Kumar, P.J. Lewis, Inhibitors of bacterial transcription initiation complex formation, ACS Chem. Biol. 8 (2013) 1972–1980.

[14] X. Yang, C. Ma, P.J. Lewis, Identification of inhibitors of bacterial RNA polymerase, Methods 86 (2015) 45–50.

[15] C. Ma, X. Yang, P.J. Lewis, Bacterial transcription inhibitor of RNA polymerase holoenzyme formation by structure-based drug design: From *in silico* screening to validation, ACS Infect. Dis. 2 (2016) 39–46.

[16] E. Andre, L. Bastide, P. Villain-Guillot, J. Latouche, J. Rouby, J.P. Leonetti, A multiwell assay to isolate compounds inhibiting the assembly of the prokaryotic RNA polymerase, Assay Drug Dev. Technol. 2 (2004) 629–635.

[17] S. Hinsberger, K. Husecken, M. Groh, M. Negri, J. Haupenthal, R.W. Hartmann, Discovery of novel bacterial RNA polymerase inhibitors: pharmacophore-based virtual screening and hit optimization, J. Med. Chem. 56 (2013) 8332–8338.

[18] B. Bae, E. Davis, D. Brown, E.A. Campbell, S. Wigneshweraraj, S.A. Darst, Phage T7 Gp2 inhibition of *Escherichia coli* RNA polymerase involves misappropriation of σ^{70} domain 1.1, Proc. Natl. Acad. Sci. U. S. A. 110 (2013) 19772–19777.

[19] T.F. Tsang, Y. Qiu, L. Lin, J. Ye, C. Ma, X. Yang, Simple method for studying *in vitro* protein-protein interactions based on protein complementation and its application in drug screening targeting bacterial transcription, ACS Infect. Dis. 5 (2019) 521–527.

[20] J. Ye, A.J. Chu, L. Lin, X. Yang, C. Ma, First-in-class inhibitors targeting the interaction between bacterial RNA polymerase and sigma initiation factor affect the viability and toxin release of *Streptococcus pneumoniae*, Molecules 24 (2019) 2902.

[21] Y. Yang, Y. Yu, X. Li, J. Li, Y. Wu, J. Yu, J. Ge, Z. Huang, L. Jiang, Y. Rao, M. Yang, Target elucidation by cocrystal structures of NADH-ubiquinone oxidoreductase of *Plasmodium falciparum* (*Pf*NDH2) with small molecule to eliminate drug-resistant malaria, J. Med. Chem. 60 (2017) 1994–2005.

[22] C. He, X. Zhang, R. Huang, J. Pan, J. Li, X. Ling, Y. Xiong, X. Zhu, Synthesis of structurally diverse diarylketones through the diarylmethyl sp3 CH oxidation, Tetrahedron Lett. 55 (2014) 4458–4462.

[23] WHO, Global priority list of antibiotic-resistant bacteria to guide research, discovery, and development of new antibiotics. https://www.who.int/medicines/publications/WHO-PPL-Short_Summary_25Feb-ET_NM_WHO.pdf, 2020 (accessed 24 June 2020)

[24] S. Watanabe, N. Takemoto, K. Ogura, T. Miyoshi-Akiyama, Severe invasive streptococcal infection by *Streptococcus pyogenes* and *Streptococcus dysgalactiae* subsp. *equisimilis*, Microbiol. Immunol. 60 (2016) 1–9.

[25] V.N. Raabe, A.L. Shane, Group B Streptococcus (*Streptococcus agalactiae*), Microbiol. Spectr. 7 (2019) 10.1128/microbiolspec.GPP3-0007-2018.

[26] G. Cammarota, A. Gallo, G. Ianiro, M. Montalto, Emerging drugs for the treatment of *Clostridium difficile*, Expert Opin. Emerg. Drugs 24 (2019) 17–28.

[27] J. Czepiel, M. Drozdz, H. Pituch, E.J. Kuijper, W. Perucki, A. Mielimonka, S. Goldman, D. Wultanska, A. Garlicki, G. Biesiada, *Clostridium difficile* infection: review, Eur. J. Clin. Microbiol. Infect. Dis. 38 (2019) 1211–1221.

[28] J. Freeman, M.P. Bauer, S.D. Baines, J. Corver, W.N. Fawley, B. Goorhuis, E.J. Kuijper, M.H. Wilcox, The changing epidemiology of *Clostridium difficile* infections, Clin. Microbiol. Rev. 23 (2010) 529–549.

[29] J. Couturier, K. Davies, C. Gateau, F. Barbut, Ribotypes and new virulent strains across Europe, Adv. Exp. Med. Biol. 1050 (2018) 45–58.

[30] S.H. Wong, M. Ip, P.M. Hawkey, N. Lo, K. Hardy, S. Manzoor, W.W. Hui, K.W. Choi, R.Y. Wong, I.M. Yung, C.S. Cheung, K.L. Lam, T. Kwong, W.K. Wu, S.C. Ng, J.C. Wu, J.J. Sung, N. Lee, High morbidity and mortality of *Clostridium difficile* infection and its associations with ribotype 002 in Hong Kong, J. Infect. 73 (2016) 115–122.

[31] D.A. Collins, K.M. Sohn, Y. Wu, K. Ouchi, Y. Ishii, B. Elliott, T.V. Riley, K. Tateda, G. *Clostridioides difficile* infection in the Asia-Pacific region, Emerg. Microbes Infect. 9 (2020) 42–52.

[32] D. Shah, M.D. Dang, R. Hasbun, H.L. Koo, Z.D. Jiang, H.L. DuPont, K.W. Garey, *Clostridium difficile* infection: update on emerging antibiotic treatment options and antibiotic resistance, Expert Rev. Anti-Infect. Ther. 8 (2010) 555–564.

[33] I. Artsimovitch, J. Seddon, P. Sears, Fidaxomicin is an inhibitor of the initiation of bacterial RNA synthesis, Clin. Infect. Dis. 55 Suppl 2 (2012) S127–131.

[34] M. Merrigan, A. Venugopal, M. Mallozzi, B. Roxas, V.K. Viswanathan, S. Johnson, D.N. Gerding, G. Vedantam, Human hypervirulent *Clostridium difficile* strains exhibit increased sporulation as well as robust toxin production, J. Bacteriol. 192 (2010) 4904–4911.

[35] M. Warny, J. Pepin, A. Fang, G. Killgore, A. Thompson, J. Brazier, E. Frost, L.C. McDonald, Toxin production by an emerging strain of *Clostridium difficile*

associated with outbreaks of severe disease in North America and Europe, Lancet 366 (2005) 1079–1084.

[36] G. Vedantam, A. Clark, M. Chu, R. McQuade, M. Mallozzi, V.K. Viswanathan, *Clostridium difficile* infection: toxins and non-toxin virulence factors, and their contributions to disease establishment and host response, Gut Microbes 3 (2012) 121–134.

[37] M.J. Aldape, D.D. Heeney, A.E. Bryant, D.L. Stevens, Tigecycline suppresses toxin A and B production and sporulation in *Clostridium difficile*, J. Antimicrob. Chemother. 70 (2015) 153–159.

[38] F. Babakhani, L. Bouillaut, P. Sears, C. Sims, A. Gomez, A.L. Sonenshein, Fidaxomicin inhibits toxin production in *Clostridium difficile*, J. Antimicrob. Chemother. 68 (2013) 515–522.

[39] M. Gerber, C. Walch, B. Loffler, K. Tischendorf, U. Reischl, G. Ackermann, Effect of sub-MIC concentrations of metronidazole, vancomycin, clindamycin and linezolid on toxin gene transcription and production in *Clostridium difficile*, J. Med. Microbiol. 57 (2008) 776–783.

[40] L.J. Drummond, D.G.E. Smith, I.R. Poxton, Effects of sub-MIC concentrations of antibiotics on growth of and toxin production by *Clostridium difficile*, J. Med. Microbiol. 52 (2003) 1033–1038.

[41] H. Yang, S. Xu, K. Huang, X. Xu, F. Hu, C. He, W. Shu, Z. Wang, F. Gong, C. Zhang, Q. Liu, Anti-staphylococcus antibiotics interfere with the transcription of leucocidin ED gene in *Staphylococcus aureus* strain Newman, Front. Microbiol. 11 (2020) 265.

[42] P.J. Lewis, S.D. Thaker, J. Errington, Compartmentalization of transcription and translation in *Bacillus subtilis*, EMBO J. 19 (2000) 710–718.

[43] X. Yang, M.J. Luo, A.C.M. Yeung, P.J. Lewis, P.K.S. Chan, M. Ip, C. Ma, First-in-class inhibitor of ribosomal RNA synthesis with antimicrobial activity against *Staphylococcus aureus*, Biochemistry 56 (2017) 5049–5052.

[44] I. Artsimovitch, M.N. Vassylyeva, D. Svetlov, V. Svetlov, A. Perederina, N. Igarashi, N. Matsugaki, S. Wakatsuki, T.H. Tahirov, D.G. Vassylyev, Allosteric modulation of the RNA polymerase catalytic reaction is an essential component of transcription control by rifamycins, Cell 122 (2005) 351–363.

[45] S. Saxena, K.K. Myka, R. Washburn, N. Costantino, D.L. Court, M.E. Gottesman, *Escherichia coli* transcription factor NusG binds to 70S ribosomes, Mol. Microbiol. 108 (2018) 495–504.

[46] T. Ren, M. Yang, M. Xiao, J. Zhu, W. Xie, Z. Zuo, Time-dependent inhibition of carbamazepine metabolism by piperine in anti-epileptic treatment, Life Sci. 218 (2019) 314–323.

[47] J. Ye, A.J. Chu, R. Harper, S.T. Chan, T.L. Shek, Y. Zhang, M. Ip, M. Sambir, I. Artsimovitch, Z. Zuo, X. Yang, C. Ma, Discovery of antibacterials that inhibit bacterial RNA polymerase interactions with sigma factors, J. Med. Chem. doi:10.1021/acs.jmedchem.0c00520

[48] D.A. Leffler, J.T. Lamont, Treatment of *Clostridium difficile*-associated disease, Gastroenterology 136 (2009) 1899–1912.

[49] Clinical & Laboratory Standards Institute, Methods for Dilution Antimicrobial Susceptibility Tests for Bacteria That Grow Aerobically, 11th Edition (M07Ed11) ed., Clinical & Laboratory Standards Institute, Wayne, PA, 2018.